https://doi.org/10.5194/egusphere-2023-61
Preprint. Discussion started: 8 March 2023

Distinct role of intraseasonal and interannual sea surface temperature anomaly in the rapid intensification onset of Typhoon Megi (2010)

Caixia Shao[1], Xidong Wang[1,2*], Kaigui Fan[1]

[1]Key Laboratory of Marine Hazards Forecasting, Ministry of Natural Resources, Hohai University, Nanjing, 210024, China

[2]Southern Marine Science and Engineering Guangdong Laboratory, Zhuhai, 511458, China

Correspondence to: Xidong Wang (xidong_wang@hhu.edu.cn)

Abstract. This study aims to explain the rapid intensification (RI) onset of Typhoon Megi from a new perspective of the intraseasonal and interannual sea surface temperature anomaly (SSTA) effect. Simulation result indicates that the warmer intraseasonal SSTA along tropical cyclone (TC) track seems to be more conducive to the early occurrence of TC RI onset than the interannual SSTA for Megi. For the experiment with intraseasonal SSTA (SST-intraseasonal), it has cooler averaged SST in TC inner-core, outer-core, and external environment than the experiment with interannual SSTA (SST-interannual). Cooler TC outer-core and environmental SST provide more midlevel radial inflow, resulting in a strong TC lower-level warm core in SST-intraseasonal. For SST-interannual, the stronger upper-level VWS related to the warmer environmental SST strongly tilts TC structure, delaying the time of RI onset. Conceptual model of Megi RI onset proposed that, when TC lower-level warm core gradually weakens and TC upper-level alignment is basically completed, TC RI onset occurs. Our results underscore the effect of intraseasonal SSTA on Megi RI onset, and provide a new perspective for improving the prediction of TC RI onset.

1 Introduction

Predicting the onset of rapid intensification (RI) of tropical cyclone (TC) is a significant challenge for the researchers and forecasters, which is mainly due to the fact that TC intensity change is linked with multiscale processes (Kaplan and DeMaira, 2003; Gall et al., 2013). Lots of studies have evidenced that the TC inner-core processes and environmental factors such as vertical wind shear (VWS), sea surface temperature (SST), relative humidity in the lower and middle troposphere, and upper tropospheric trough forcing all can influence the RI of TC (Emanuel et al., 2004; Maclay et al. 2008; Elsberry et al., 2013; Montgomery et al., 2013; Rogers et al., 2015). Although large effort has been made to elucidate the physical mechanisms governing TC inner-core processes and their interaction with the large-scale environment, our understanding

https://doi.org/10.5194/egusphere-2023-61
Preprint. Discussion started: 8 March 2023

about RI onset still remain inadequate (Smith and Montgomery, 2015). In order to simplify such a complex processes, a useful conceptual of TC RI onset has always been sought. Especially for the strong destructiveness of unexpected RI of strong TCs close to the coast, the need for improving our understanding of TC RI is underscored (Kaplan and DeMaria, 2003).

SST is considered to be an important factor for TC intensity that directly determines the heat fluxes at the air sea interface beneath the TC (Emanuel, 1986; Holland, 1997). Presumably, when the SST is higher, the moisture flux at the air sea interface may be larger, which is conducive to the intensification rate of TC (Shay et al., 2000; Črnivec, et al., 2016; Xu and Wang, 2018). Kaplan and DeMaria (2003) investigated the SST condition for RI TCs in North Atlantic, and found that the mean SST for TCs with RI was higher than that of non-RI TCs. Also in the WNP, many RI TCs happened in the regions with higher SST (Wang et al., 2015). In addition, the energy extracted effectively by TC is much smaller than the energy available, and the SST under TC inner-core region seems to be the crucial factor for TC intensity evolution (Emanuel, 1999; Cione and Uhlhorn, 2003). Some researchers focused on the influence of SST on the dynamic process in TC inner-core region, where there was a high symmetry of precipitation around the eyewall region when the RI onset occurs (Rogers, 2010; Chen et al., 2018). Therefore, the local region with higher SST associated with the warm ocean eddies may be a vital potential energy source for TC RI onset (Chan et al.,2001; Shay et al., 2000; Hong et al., 2000; Ma et al., 2017). In addition, the influence of outer-core SST on TC intensity has also been explored, giving a result of that the higher SST there inhibited the TC intensification (Sun et al., 2014; Kanada et al., 2017), consistent with the negative role of higher surface entropy fluxes of outer-core region in TC intensity found by Xu and Wang (2010). A suggestion of this inhibiting effect is that the higher SST outside the effective radius (about 1.5-2.0 times the RMW) promotes more surface enthalpy flux into the outer spiral rainbands and less surface enthalpy flux into the eyewall (Sun et al., 2014). The foregoing studies help us understand the conceptual theory of local SST's effect on TC intensity. More detailed studies are needed to explain how the environmental SST affect the RI onset when simultaneously adjusting the TC inner-core, outer-core and atmospheric environment factors.

With climate warming, both the observed and modeled results have demonstrated that the frequency of RI TCs significantly increase in Atlantic and WNP, which makes TC intensity forecasting more difficult (Emanuel, 2017; Mei and Xie, 2017; Bhatia et al., 2019). One of the ways to solve this difficulty is to fully consider the multiscale air-sea interaction related to TC intensity change. For a few decades, the full consideration has been taken into in the medium range and seasonal forecasts of TC. The intraseasonal and interannual factors which affect both the local heat fluxes and environmental parameters during TC period gradually received attention (Vitart and Robertson, 2018; Singh et al., 2021). In addition, there are some distribution characteristics of RI's frequency and location at intraseasonal and interannual timescales (Wang and Zhou, 2007; Wang et al., 2015; Wang et al., 2017), which means that there may be a certain correlation between TC RI and different timescale ocean oscillation. This is also enlightening for the improvement of short-term forecasting of TC, and makes us pay attention to the role of different timescale SSTA in TC RI onset.

https://doi.org/10.5194/egusphere-2023-61
Preprint. Discussion started: 8 March 2023

Recently, some research focused on the RI process of the super Typhoon Megi in 2010 (Wang et al., 2014; Fang and Zhang, 2016; Chang and Wu, 2017; Lee and Wu, 2018; Chang et al., 2020) and the air-sea interaction in TC region during the RI period (D'Asaro et al., 2014; Wu et al., 2016; Kanada et al., 2017; Pun et al., 2018). The RI of Megi occured in the mid-autumn of a strong La Niña year (2010), and Megi moved fast and intensified to a super typhoon in very short time. Based on the observed and modeled results, the La Niña-like cooling pushes the TCs generation westward, with the favorable ocean thermodynamic environment for the TC intensification in Western Tropical Pacific (Zhao et al., 2018). Ge et al. (2018) found that ocean thermal condition in October promotes the TCs RI in WNP, when the RI ratio is greatest. Meanwhile, there is obvious intraseasonal SSTA signal in WNP (Ren et al., 2013), where Megi passes. The SSTA is closely related to the large-scale atmospheric circulation (Ren et al., 2013) and vertical wind shear (VWS, Latif et al., 2007), which directly determines the environmental conditions around TC (Riemer et al., 2013; Tao and Zhang, 2019). As is found by Camargo et al. (2009) and Chen et al. (2018), the intraseasonal oscillation either constructively or destructively interfere with the impact of ENSO on TC activity and development in North Atlantic and WNP. As the intraseasonal and interannual ocean signal occur simultaneously, it is valuable to investigate the role of the intraseasonal and interannual SSTA in Megi's RI onset, which is still poorly known.

The remainder of this paper is structured as follows. Section 2 introduces the model configuration and verification of the control and sensitive simulation. Section 3 quantitatively analyze the intraseasonal and interannual SSTA contribution to Megi's RI onset. Section 4 presents the TC thermodynamic modification by different SSTA. Section 5 shows the effect of SSTA on the thermodynamic processes associated with the RI onset, and Section 6 gives the discussion and a brief summary.

2 Model configuration

2.1 Observed RI of Typhoon Megi

A RI event is defined as when the maximum sustained wind speed increases by more than 30 kt over a period of 24 h (Kaplan and DeMaria, 2003). Based on the RI definition, Typhoon Megi (2010) experienced a typical RI period before landing Luzon Island (Fang and Zhang, 2016; Chang and Wu, 2017). According to the observed typhoon intensity data from Joint Typhoon Warning Center (JTWC), the RI phase of Megi started from 00 UTC 16 October to 12 UTC 17 October, with the maximum wind speed (MWS) increasing from 90 kt to 160 kt, and the central sea level pressure (CSLP) dropping from 956 hPa to 903 hPa. Referring to the metric used in the study of Tao et al. (2017), Megi's intensification period is divided into two stages, namely, "before RI" (0-24 h before RI onset), and "during RI" (from the RI onset to the time of TC reaches the peak intensity), and RI onset is the starting time of the RI (00 UTC 16 OCT).

2.2 SST and SSTA distribution during Megi

Referring to the method adopted by Krishnamurthy and Shukla (2000), the original daily SST (from NOAA OI SST V2 High Resolution Dataset) is considered to be the sum of high frequency SST fluctuation, daily SST climatology, intraseasonal

https://doi.org/10.5194/egusphere-2023-61
Preprint. Discussion started: 8 March 2023

SSTA, and interannual SSTA. The high frequency fluctuation in the original daily SST is removed by applying a 5-day running mean. The daily SST climatology developed from OISST data for the period of 1982-2010. After removing the high frequency fluctuation and daily SST climatology from the original daily SST, the interannual SSTA is obtained by averaging the residual SST from 1th SEP to 30th NOV in 2010. We therefore get the daily intraseasonal SSTA by removing the above three terms from daily SST.

Typhoon Megi forms in the tropical ocean east of Philippine archipelago, and then fast moves west-northward to the Northwest Pacific Subtropical Countercurrent (STCC) area, where there is a pronounced SST front in winter (Kobashi and Kubokawa, 2012). When Megi arrives around the southern periphery of STCC, the RI onset occurs and Megi turns to west-southwestward toward Luzon Island. Along Megi track, the SST is much higher than 29℃ (Fig. 1a). Meanwhile, the positive intraseasonal SSTA is distributed near Luzon Island and Kuroshio area (Fig. 1d). As Megi happens in the autumn of a strong La Niña year (2010), there is a positive interannual SSTA over the WNP (Fig. 1e). Difference between intraseasonal and interannual SSTA indicates that the positive interannual SSTA signal mainly presents a large-scale average distribution in TC passing area, and the positive intraseasonal SSTA is relatively concentrated along TC track. Before RI, the positive interannual SSTA around TC track is stronger than intraseasonal SSTA. During RI, the stronger positive intraseasonal signal is mainly distributed on the north side of the TC track, and the stronger positive interannual SSTA mainly occurs on the south side (Fig. 1d-f). Therefore, the warmer SST with intraseasonal signal (without interannual SSTA) is concentrated around TC track and gradually decreases outward (Fig. 1b). After the intraseasonal SSTA is removed, the distribution of the residual SST with interannual signal is much higher in the southeast and lower in the northwest of Western Tropical Pacific (Fig. 1c).

2.3 Model configuration of experiment

A high-resolution atmosphere model (WRF) is used here to reproduce the RI of Megi, integrating from 06 UTC 15 OCT to 00 UTC 19 OCT. In control simulation forced by the original SST (hereafter referred to as CTRL), there are three nests in WRF which are set at 18, 6 and 2 km resolutions, and the third nest is a vortex-following moving grid. There are 55 vertical levels with the top set at 30 hPa. The double-moment SBU-YLIN cloud microphysic scheme is used to predict the mass mixing ratios (Lin and Colle, 2011), and GFS Simplified Arakawa-Schubert cumulus parameterization scheme is applied for domain 1 and 2 (Bassill, 2015). The planetary boundary layer scheme is Grenier-Bretherton-McCaa (Bretherton and Park, 2009). Modeling initial and lateral boundary conditions and updated SST force fields come from the Global Forecast System (GFS) final analysis (FNL) dataset and NOAA OI SST V2 High Resolution daily dataset, respectively.

To examine the contribution of intraseasonal and interannual SSTA to Megi's RI onset, the sensitivity experiments (hereafter refer as SST-intraseasonal and SST-interannual) are proposed. Their atmospheric module settings is the same as that of the CTRL. In particular, SST-intraseasonal uses the SST field (shown in Fig. 1b) including the daily SST climatology, high

https://doi.org/10.5194/egusphere-2023-61
Preprint. Discussion started: 8 March 2023

frequency SSTA and intraseasonal SSTA to force atmospheric simulation. For SST-interannual, the SST field is the combination of daily SST climatology, high frequency SSTA and interannual SSTA (Fig. 1c).

3 Overview of the numerical experiments

3.1 Verification of the numerical experiments

Figure 2 compares Megi intensity and track of the numerical experiments with observed JTWC data. Figure 2a shows that TC CSLP evolution is reasonably simulated by CTRL with approximately 5.2 hPa of 84 h (from 12 UTC 15 OCT to 00 UTC 19 OCT) mean intensity error. For the simulated MWS, the 84 h mean error relative to the JTWC MWS is 9.65 kt, and the RI onset in CTRL occurs 6 h later than the observed result (00 UTC 16 OCT in JTWC and 06 UTC 16 OCT in CTRL). Thus the "before RI", and "during RI" in CTRL is defined as the period from 06 UTC 15 OCT to 06 UTC 16 OCT, and from 06 UTC 16 OCT to 12 UTC 17 OCT, respectively. The 84-h mean track error is approximately 59.6 km, with the biggest deviation (191.8 km) occurs at 00 UTC 18 OCT, when Megi is close to the Luzon Island. Here, the CTRL run is used as a benchmark to assess the impact of SSTA.

Regarding the CTRL and sensitive simulated intensity evolution, it is presented in Fig. 2a that TC CSLP in all experiment shows a continuous decreasing trend from 06 UTC 16 OCT to 00 UTC 18 OCT. Based on the evolution of TC MWS, the RI onset of SST-intraseasonal and SST-interannual occurs at 00 UTC and 12 UTC on 16 OCT, which is 6 h earlier and 6 h later than CTRL, respectively. The TC peak MWS happens at 00 UTC18 OCT in SST-intraseaonal and SST-interannual, 12h later than CTRL. The contribution of SSTA to the simulated tracks is relative small (Fig. 2c).

3.2 Evolutions of the mean SST and heat flux

As the actual SST distribution during TC track is complicated, the imposed SST and heat flux caused by intraseasonal and interannual SSTA is assessed through different TC radial ranges. To facilitate the intercomparison of the SST evolution in each experiment, the mean value of SST and heat flux in TC inner-core region here is defined as the average value within a radius of 0-100 km, and the outer-core and environmental mean value is averaged from radius of 100-200 km and 200-800 km, respectively. Heat flux is the sum of sensible heat flux (SHX) and latent heat flux (LHX), which are from model output directly.

Figure 3 compares the mean SST and heat flux within different TC regions among the various experiments. Apparently, the mean SST and heatflux in TC inner-core, outer-core and environmental in CTRL is larger than those in SST-intraseasonal and SST-interannual during the whole simulated period. Comparing SST of the twain sensitive experiments, SST-interannual is significantly warmer than SST-intraseasonal before their RI onset in the various regions (Fig. 3a-c). While the difference of mean heat flux in TC inner-core between the twain experiments oscillates from 00 UTC 16 OCT to 00 UTC 17 OCT (Fig. 3d). The mean outer-core and environmental heat flux in SST-interannual is larger than SST-intraseasonal before RI (Fig. 3e-f).

https://doi.org/10.5194/egusphere-2023-61
Preprint. Discussion started: 8 March 2023

Above comparison indicates that although SST-intraseasonal has cooler SST and lesser heat flux in TC inner-core than CTRL and SST-interannual before RI, the RI onset of SST-intraseasonal is the earliest. Thus the contribution of inner-core and outer-core SST to Megi RI onset needs to be further explored. Sun et al. (2014) has mentioned that the warmer SST inside inner-core region (about 1.5-2.0 times the RMW) can promotes TC intensification, contrasted with the opposite effect in the outer region (from 2.0 time the RMW to 255km). Therefore, both TC inner-core, outer-core and environmental SST factors should be considered together to investigate the impact of SSTA on TC RI onset. The following sections will give a detailed description about the analysis.

4 TC thermodynamic modification by SSTA

The effect of intraseasonal and interannual SSTA on TC thermodynamic modification related to RI onset is analyzed in an axisymmetric view in this section. Riemer et al. (2010, 2013) have presented that there is a tongue of low potential temperature (low-θ) air intruding into the inflow layer from the above and radially inwards towards the eyewall after the VWS is imposed. Based on the axisymmetric spindown theory, the substantial decrease of the convective mass flux associated with the cooler inflow layer potential temperature induces the TC rapid weakening (Elliassen and Lystad, 1977; Montgomery et al., 2001). In addition, when the inflow layer θ is replenished, TC re-intensification occurs (Riemer et al., 2013). These previous studies can help us understand the TC spindown process under VWS. Here, we try to explain the effect of SSTA distribution on TC RI onset based on the above-mentioned theoretical basis.

4.1 Evolution of the two-level warm cores

TC warm core is one of the typical thermodynamic structure during TC period. The upper-level warm core has been explored in some studies, which indicates that it associates with TC RI (Chen and Zhang, 2013). Figure 5 shows that the two warm cores with the warming center upon the TC eye is at about 4 km and 14 km height, respectively. Lower-level warm anomaly happens earlier than the upper-level one for the three experiments, consistent with the findings of Tao and Zhang (2019). Tao and Zhang (2019) also pointed out that after the TC RI onset, the two-level warm cores gradually merge. For Megi, the different SST configuration cause different time of RI onset and two-level warm cores connection. In CTRL, RI onset is at 06 UTC 16 OCT, and the connecting channel between the two-level warm cores is gradually opened at 12 h after the RI onset (18 UTC 16 OCT). The above two time nodes in SST-intraseasonal are 00 UTC 16 OCT and 00 UTC 17 OCT. For SST-interannual, the RI onset is at 12 UTC 16 OCT, and upper-level warm core begins to merge with lower one at 00 UTC 17 OCT. It indicates that SST has influenced both TC lower-level and upper-level structures. The lower-level warm center occurs earlier than TC RI onset, and gradually weakens nearly before RI onset. The peak intensity of TC upper-level warm core in CTRL and SST-intraseasonal is warmer than SST-interannual, corresponding well to TC peak intensity in each experiment. Our results imply that the lower-level warm core is more likely to be an indicator of TC RI onset than the upper-level warm core. Next, we explore how the SST distribution affects TC two-level warm cores and what is the relationship between TC warm cores and RI onset. More analysis about the evolution of TC thermodynamic structure is needed.

https://doi.org/10.5194/egusphere-2023-61
Preprint. Discussion started: 8 March 2023

4.2 TC ventilation structure and vertical wind shear

Figures 5-7 depict the evolution of two-level warm cores in each experiment under environmental VWS prior to and during TC RI. Generally, before RI from 12 UTC 15 OCT to 00 UTC 16 OCT, the lower-level warm core reaches a relatively strong state earlier than the upper-level one, consistent with the result shown in Fig. 4. It is well known that the higher inner-core SST is benefit for the development of TC inner-core convection, which is closely related to TC intensity. Our results indicate that, although the averaged inner-core SST in SST-intraseasonal is lower than the other experiments, its lower-level warm core is as strong as those in CTRL and SST-interannual (Figs. 5g-i).

The difference of ventilation structure is a typical topics to start the exploring, which is closely related to VWS and TC outer-core SST. Previous studies have proved that the dry and strong VWS environment can cause two-level radial ventilation structures for a weaker TC documented based on both modeling and observational case studies (Riemer and Montgomery, 2011; Alland et al., 2021). The lower-level ventilation is located between sea surface to middle troposphere with rainband activity and downdraft ventilation, and the upper-level one aloft is associated with TC vertical tilting (Alland et al., 2021). Figures 5-6 show that, during the period before RI when TC is weaker, the two-level TC ventilation structures gradually appear, corresponding to the two-level warm cores inside TC inner-core region. The lower-level ventilation structure is at the height of about 0-8km, and the upper one is at about 8-16km. TC lower-level and midlevel radial cooling band in each ventilation locates at about 2-4km and 8-10km height, respectively, which involves the dilution of warm air in TC inner-core with cooler air intruding from the environment outside TC. Comparing TC radial cooling effect, Fig. 5e shows a stronger lower-level cooling in SST-intraseasonal than those in Figs. 5d-f. For the upper-level radial cooling, stronger cooling band in the SST-intraseasonal locates outside TC eyewall, but the other experiments' cooling bands flush into TC inner-core. Therefore CTRL and SST-interannual have a larger tilting to exhibit the upper-level warm core moving to near the eyewall. One of the reasons for the stronger cooling of SST-intraseasonal is due to its relatively cold outer-core SST. Sun et al. (2013) has shown that TC outer-core mixing of convection by warmer outer-core SST reduces the radial inflow towards TC eyewall. The cooler outer-core SST therefore promotes the lower-level radial cooling, which also induces more radial angular momentum input.

For VWS, some studies have demonstrated that the deep-layer shear (200-850 hPa) alone is not sufficient for understanding the effect of VWS on TCs (Finocchio et al., 2016; Onderlinde and Nolan, 2014). Upper-level and lower-level VWS have been separately utilized to analyse the modulating effect of VWS on TC intensity (Finocchio et al., 2016; Gao et a., 2020). Based on the idealized numerical simulations, Finocchio et al. (2016) point out that the lower-level shear promotes the advection of midlevel thermodynamically unfavorable air, which is detrimental to TC intensity, and the upper-level shear is more favorable for TC intensification with less downdrafts flush the boundary layer. Gao et al. (2020) have found that the upper-level shear tends to produce a stronger asymmetric outflow at upper levels than lower-level shear, transporting more water vapor outward at upper levels. For a realistic TC simulation, the upper-level and lower-level shear act simultaneously. Based on the characteristic of Megi's ventilation structure, we get the upper-level shear by calculating large-scale wind shear

https://doi.org/10.5194/egusphere-2023-61
Preprint. Discussion started: 8 March 2023

between 14 km and 8 km height averaged from radii of 200 km to 800 km, and the lower-level shear is calculated based on large-scale shear between 8 km and 2 km height. Result shown in Fig. 8 indicates that, during the period of before RI, all the three lower-level shear experience a trend of decreasing first and then increasing. Earlier before TC RI, the lower-level shear of SST-intraseasonal is the strongest, followed by SST-interannual and CTRL. Contrary to the lower-level shear, the order of upper-level shear is CTRL, SST-interannual and SST-intraseasonal. After 00 UTC 16 OCT, the lower-level shear decreases rapidly, but the upper-level shear keeps increasing for a period. Above analysis demonstrates that, the cooler environmental SST in SST-intraseasonal corresponds with a stronger lower-level shear and a weaker upper-level shear before RI.

To explore the effect of two-level shear, we connect the evolution of TC ventilation structure and VWS. Before Megi RI onset, the midlevel cooling band flushes the upper-level warm core in CTRL and SST-interannual (Fig. 5d, f), in which there is a stronger upper-level shear than SST-intraseasonal (Fig. 8a). The stronger upper-level shear induces more cooler environmental air intruding into the center of upper warm core to obviously increase TC tilting (Fig. 5i). However, SST-intraseasonal has a relative weaker upper-level shear with a cooling band outside TC upper-level eyewall. Comparing the lower-level shear, SST-intraseasonal has the strongest lower-level shear to maintain TC ventilation structure and bring more angular momentum input. In addition, cooler outer-core SST in SST-intraseasonal is conductive to the maintenance of TC ventilation structure. Especially, when the lower-level cooling band is gradually replaced by the warming effect and upper-level TC alignment is basically completed, TC starts to rapidly strengthen (Figs. 6a, 5h and 6f). When TC comes to its RI stage, there is an obvious growing upper-level warm core (Figs. 6-7). Those processes result in that TC lower-level warm core in SST-intraseasonal is as strong as the other two experiments. This enlightens us that a moderately weaker upper-level shear and stronger lower-level shear is conducive to the occurrence of TC RI onset, under which TC has a relative less tilting and more lower-level radial inflow entering.

According to the above analysis, the influence of SST on TC RI onset is reflected both in the development of TC warm cores and the adjustment of ventilation structures. Warmer TC inner-core SST promotes the generation of convection near TC eyewall, and cooler outer-core SST and stronger lower-level VWS correlates with cooler environmental SST improve more external angular momentum input. Therefore, it can be understood that although inner-core SST of SST-intraseasonal is lower than CTRL and SST-interannual, SST-intraseasonal has a strong lower-level warm core by its cooler outer-core SST and stronger lower-level VWS. For CTRL and SST-interannual, the stronger upper-level VWS delays TC RI onset when the midlevel radial inflow extends to TC inner-core region. Thus CTRL and SST-interannual take more time to consume TC upper tilting structure. Generally, TC RI onset is the result of TC thermodynamic structure adjustment and interaction with external environment, which could be predicted by using the indicator of the modulation of TC lower-level warm core, ventilation structure and upper-level alignment. The effect of TC inner-core, outer-core and environmental SST on Megi RI onset should be considered simultaneously.

https://doi.org/10.5194/egusphere-2023-61
Preprint. Discussion started: 8 March 2023

5 Thermodynamic processes associated to Megi RI onset

As discussed above, Megi RI onset crucially depends on the match of TC heating against the radial ventilation cooling. Qualitatively exploring the affect of SSTA on TC heating process could further improve our understanding of SST's contribution to TC RI onset.

Potential temperature budget analysis is conducted to identify how the imposed SST impact on the radial distribution of the potential temperature variation, that is,

$$\frac{d\theta}{dt} = \mathrm{COND} + \mathrm{HEAT} + \mathrm{RAD} + \mathrm{RESI}\ , \quad (1)$$

Where θ, COND, HEAT, RAD, and RESI is potential temperature, condensation-induced heating, latent heating, radiation heating, and diffusion term, respectively. Decomposing the quantities of Eq. (1) into azimuthal mean and perturbation components, the azimuthally averaged potential temperature budget in cylindrical coordinates can be obtained as

$$\frac{\partial\overline{\theta}}{\partial t} = \left(-\overline{u}\frac{\partial\overline{\theta}}{\partial r} - \overline{u}' - \frac{\overline{v}'}{r}\frac{\partial\overline{\theta'}}{\partial\lambda}\right) + \left(-\overline{w}\frac{\partial\overline{\theta}}{\partial x} - \overline{w'}\frac{\partial\overline{\theta'}}{\partial z}\right) + COND + HEAT + RAD + RESI\ , \quad (2)$$

where the overbar and prime are the azimuthal mean and perturbation components, respectively; θ is the potential temperature, u, v, and w are the radial, tangential and vertical wind velocities in the cylindrical coordinate system (r, λ, z), t is time. The term on the left-hand side is the azimuthally averaged potential temperature tendency. The right-hand side terms represent the contributions of the horizontal advection (HADV), vertical advection (VADV), condensation-induced heating (COND), PBL heating (PBL), radiation heating (RAD) and the diffusion (RESI), respectively (Ma et al., 2015). The COND, PBL and RAD are directly from the model output, and RESI is the residual term. Here, TC heating processes at lower, middle and upper altitude (4, 8, and 14 km) is examined, and the qualitative explanation is provided.

Figure 9 shows the potential temperature evolution at 4 km, 8 km and 14 km for the three experiments. At 4 km height of each experiment, there is a warming $\overline{\theta}$ band extending from TC inner-core to outer-core nearly after 12 UTC 15 OCT. The warming effect is closely related to TC ventilation structure, which hinders TC lower-level convective motion. After the warming effect is nearly complete, SST-intraseasonal's RI onset occurs. As it is described in Sec. 4, the delay of RI onset in CTRL and SST-interannual is owed to TC upper-level tilting. Figures 9 d-f show a TC cooling band at 8 km height after 12 UTC 15 OCT for the three experiments, and then a warming band occurs nearly after 00 UTC 16 OCT. Comparing three experiments, the outer-core warming effect in CTRL and SST-interannual is stronger than SST-intraseasonal, related to the stronger ventilation structure at 8km in CTRL and SST-interannual preserving TC released heat. At 14 km height where the upper warm core locates, SST-interannual has the strongest TC cooling effect inside inner-core at around 18 UTC15 OCT (Fig. 9i), corresponding with its strongest radial cooling (Fig. 5f, i).

https://doi.org/10.5194/egusphere-2023-61
Preprint. Discussion started: 8 March 2023

5.1 Potential temperature budget analysis at 4 km

Next, the potential temperature budget analysis at TC 4 km-level is provided to get a deeper understanding about TC lower-level thermodynamic processes. Figures 10 and 11 depict the contribution of budget terms to local $\overline{\theta}$ tendency at the height of 4 km. During the period before RI, TC lower-level warm core is mostly caused by the contribution of COND, HADV, and RESI term, which is related to the effect of rainband heating, horizontal advection heating, and diffusion heating, respectively. TC outer-core warming band is caused by the effect of COND, HADV, and RAD. COND′s heating effect almost covers all areas inside TC region, corresponding to the active lower-level convection both in TC inner-core and outer-core region. HADV warming effect concentrates inside TC eye region, playing a negative role outside TC eyewall related to the cooling radial inflow from outer region. Due to the cooling zone below TC 4 km-height, VADV plays a negative role in most areas of TC region. RESI is manifested in heating inside TC eyewall and cooling outside the eyewall. RAD and PBL shows a weak cooling effect in TC inner-core and a weak warming effect in TC outer-core.

Figures 12 and 13 quantitatively presents averaged contribution of each thermodynamical term to TC lower-level $\overline{\theta}$ in TC inner-core and outer-core, respectively. Before RI, the positive contribution to lower-level inner-core warming is mostly from RESI and COND terms (Fig. 12c and d), and negative contribution is mostly from HADV, VADV, and PBL (Fig. 12a, b and e). Although inner-core SST in SST-intraseasonal is cooler than CTRL and SST-interannual, the averaged rainband heating (COND) in SST-intraseasonal is the largest from 12 UTC to 15 UTC 15 OCT and from 21 UTC 15 OCT to 03 UTC 16 OCT (Fig. 12d). COND′s warming process is the vital factor for SST-intraseasonal to obtain a stronger lower-level warm core. This corresponds to the result shown in Sec. 4, which indicates that stronger radial input can promote convection in TC inner-core region. Finally, all above processes lead to TC averaged $\overline{\theta}$ experiencing a first increasing and then decreasing trend from 12 UTC 15 OCT to 00 UTC 16 OCT (Fig. 12f). After TC inner-core sharper cooling is nearly complete, SST-intraseasonal enters its RI onset immediately.

Figure 13 compares the contribution of each budget term to TC outer-core $\overline{\theta}$ tendency at 4 km height. For SST-intraseasonal, the positive contribution is from HADV, RESI, and COND, and negative contribution is mostly from VADV. For CTRL and SST-interannual, HADV and COND plays positive roles in $\overline{\theta}$ warming, in contrast with the negative effect of VADV and RESI. The largest positive and negative contributions in all three experiments are from COND and VADV, respectively. Figs. 13b and 13d show that, SST-intraseasonal has the weakest COND warming effect in TC outer-core region, which is benefit for more midlevel radial inflow towards to TC inner-core. In addition, less VADV cooling and more RESI warming make SST-intraseasonal produce a similar outer-core warming effect with the other experiments. Generally, TC outer-core averaged $\overline{\theta}$ presents a increasing trend before 00 UTC 16 OCT (Fig. 13f), corresponding to the weakening trend of lower-level radial cooling before TC RI.

In conclusion, there is a significant radial warming band at 4 km height of TC region during and before RI, when environment provides a strong VWS outside the TC. The radial warming band is mainly caused by the condensation heating

https://doi.org/10.5194/egusphere-2023-61
Preprint. Discussion started: 8 March 2023

of lower-level rainband, which has a large spatial coverage. Although SST-intraseasonal has the lowest inner-core and outer-core SST, the lower-level warming effect both in inner-core and outer-core is as strong as the other experiments. Especially, SST-intraseaonal has less convection in TC outer-core region, which induces more convection in TC inner-core due to more radial inflow flushing into TC inner-core. When TC lower-level warming process is nearly complete, there is an obvious cooling trend in TC inner-core. This is consistent with the result found by Tao and Zhang (2019), who presents an evidence of the cooling effect before RI. CTRL and SST-interannual also show a cooling process around 00 UTC 16 OCT, but its RI onset is 6h and 12h later than SST-intraseasonal. As mentioned in Sec. 4, the stronger upper-level VWS of CTRL and SST-interannual puts TC upper-level structure more tilted, which prolongs the period of TC alignment. Therefore, we will further analyze TC $\overline{\theta}$ evolution at 8 km to understand the delay of RI onset.

5.2 Potential temperature budget analysis at 8 km

At 8 km height of TC region, there is a cooling band earlier before TC RI, following with a warming band (Fig 9d-f). Figures 14-15 shows TC potential temperature budget contribution at 8 km. It indicates that the effect of HADV, VADV and RESI term in CTRL is obvious different from the other experiments, because of CTRL's lower-level warm core and outer-core warming band extends to a higher TC level. Comparing SST-intraseasonal and SST-interannual, the warming contribution is mostly from COND, RAD and RESI, and cooling effect is mostly from VADV, PBL, and HADV. Figure 15 compares the budget terms in TC inner-core at 8km, and shows that SST-intraseasonal has significantly more COND heating contribution than SST-interannual before 09 UTC 16 OCT (Fig. 16). This may be due to the fact that the ventilation structure of SST-interannual destroys TC upper-level warm core. While the cooling effect of VADV in SST-intraseasonal is stronger than SST-interannual. All above contributions result in a more obvious cooling process from 12 UTC to 18 UTC 15 OCT and a stronger warming process from 18 UTC 15 Oct to 00 UTC 16 OCT in SST-intraseasonal. TC inner-core warming in SST-interannual is stronger than SST-intraseasonal from 00 UTC to 06 UTC on 16 OCT, when SST-interannual is repairing its upper-level inner-core structure.

TC outer-core averaged effect of budget terms is shown in Fig. 17, which indicates that VADV and COND are also the vital factors determining $\overline{\theta}$ change. Before 00 UTC 16 OCT, SST-intraseasonal has wearker COND warming effect and weaker VADV cooling effect than SST-interannual, consistent with SST-intraseasonal's stronger outer-core cooling process. At 00 UTC 16 OCT, SST-intraseasonal's RI onset occurs, while CTRL and SST-interannual need to further adjust TC upper-level structure. TC outer-core $\overline{\theta}$ in CTRL and SST-interannual experience a strong increasing trend from 00 UTC to 06 UTC on 16 OCT nearly before their RI onset, to resist the strong midlevel inflow and continue TC alignment.

Generally, for TC $\overline{\theta}$ at 8 km height, there is a significant radial cooling band mainly due to VADV cooling effect both in TC inner-core and outer-core region. For SST-intraseasonal, when the cooling process is nearly complete, TC RI onset occurs. For CTRL and SST-interannual, although their cooling process is complete, their TC upper-level tilt prolongs the period of

https://doi.org/10.5194/egusphere-2023-61
Preprint. Discussion started: 8 March 2023

TC alignment. The role of SST inTC atmosphere at 8 km height is reflected in its impact on TC upper-level tilting. As lower ambient SST of SST-intraseasonal is corresponding to a weaker upper-level shear than CTRL and SST-interannual, SST-intraseaonal has the weaker tilting and spends shorter time to modulate TC structure before RI.

6 Discussion and conclusion

Significant intraseasonal and interannual SSTA exist in WNP where TCs pass across. The role of different scale SST in TC RI onset remains unclear. This study therefore investigates the evolution of typhoon Megi's thermodynamic processes prior to RI forced by different scale SST using modeling experiments. By comparing SST distribution in control and sensitive experiments, SST-intraseasonal experiment containing intraseasonal SSTA signal has the coolest averaged SST all in TC inner-core, outer-core and external environment region, but Megi RI onset in SST-intraseasonal experiment is 6h and 12 h earlier than CTRL and SST-interannual, respectively. To give a comprehensive explanation about different scale SSTA's contribution to Megi RI onset, our study deeply explores the relationship between intraseasonal, interannual SSTA and TC thermodynamic structure evolution.

Process about the effect of intraseasonal and interannual SSTA on Megi′s RI onset is summarized in Figure 18. Before RI onset, there are two-level ventilation structures within TC Megi closely related to the two-level VWS, with two obvious cooling band outside the eyewall (Figs. 18a-b, e-g). TC inner-core warm effect produces an obvious lower-level warm core (center at about 4 km height), compared with the outer-core warming offsetting the ventilation cooling. When TC lower-level warm core gradually weakens and TC upper-level alignment is basically completed, TC RI onset occurs (Figs. 18c-d, h). Before RI, TC $\overline{\theta}$ at 4km and 8km height experience a warming and cooling process, respectively. The comparison of three experiments′ lower-level $\overline{\theta}$ evolution indicates that SST-intraseasonal′s lower-level warming effect in TC inner-core is as strong as the other experiments. We demonstrate that the cooler outer-core SST and stronger lower-level VWS by cooler environmental SST brings more angular momentum input, resulting in more condensation warming in TC inner-core. For TC upper-level structure, the weaker upper-level VWS in SST-intraseasonal induces a weaker TC upper-level tilt than the other experiments. And the cooling effect at 8km height is caused by midlevel radial inflow, which extends to TC upper-level inner-core in CTRL and SST-interannual. For SST-intraseasonal, when the warming process at 4km and cooling process at 8km is nearly completed, TC RI onset occurs. For CTRL and SST-interannual, they spend more time on TC upper-level alignment.

Our result indicates that a strong TC lower-level warm core and TC upper-level alignment should be considered as the indicators of TC Megi RI onset. Because TC lower-level warm core represents that TC keeps developing under high VWS, and the stronger TC upper-level tilting may delay the RI onset. Thus we should consider both TC lower-level and upper-level thermodynamic modification simultaneously when predicting the RI onset.

https://doi.org/10.5194/egusphere-2023-61
Preprint. Discussion started: 8 March 2023

Recent work has indicated that strong VWS is considered as a hostile environmental impact factor on TC intensification, because it can lead to the emergence of TC ventilation structure. However, based on the analysis in this study, the hypothesis put forward is that relatively high lower-level VWS in SST-intraseasonal is beneficial to TC Megi RI onset. This phenomenon has also been mentioned in previous studies. For example, the result shown in Tao and Zhang (2019) indicates that TC RI only happens when the VWS is relatively high. And Liu et al. (2022) points out that the stronger shear is more favorable for TC secondary eyewall formation than the weaker shear when the shear magnitude is smaller than 15 ms-1. Based on the analysis of two-level TC warm cores and ventilation structure, we find that the stronger lower-level VWS may bring more high angular momentum environmental air towards into TC inner-core. The stronger ventilation radial inflow promotes more convective systems inside TC inner-core region earlier before RI onset, and TC gradually accumulates energy and adjusts its structure to cope with shear environment. The decreasing lower-level VWS during RI period is due to the feedback of TC enhancement, but not a cause of TC intensification.

In conclusion, the intraseasonal SSTA along TC track seems to be more conducive to the early occurrence of TC RI onset than interannual SSTA for Megi. Our result underscores that the effect of TC inner-core, outer-core and environmental SST on TC RI onset should be considered simultaneously. In addition, the conceptual model we proposed may provide a new perspective for improving the prediction of TC RI. Analysis provided here is in the sight of TC axisymmetric thermodynamic structure and processes prior to TC RI, dynamic processes and symmetric thermodynamic processes will be presented in our future study.

Author contributions. CS is responsible for the entire project, including modifying the parameterization scheme of the numerical simulations, analyzing the simulation result, and drafting the manuscript. XW provides many suggestions, insights, and discussions on the manuscript draft and paper revisions. KF partly contributes to the data analysis of this work.

Acknowledgments

This study is supported by the Special Founds for Creative Research (2022C61540), the National Natural Science Foundation (41776004), and the Opening Project of Key Laboratory of Marine Environmental Information Technology (20195052912). K. Fan is also supported by the Postgraduate Research & Practice Innovation Program of Jiangsu Province (KYCX21_0450) and the scholarship from China Scholarship Council (202106710089).

https://doi.org/10.5194/egusphere-2023-61
Preprint. Discussion started: 8 March 2023

References

Bassill, N. P.: An analysis of the operational GFS simplified Arakawa Schubert parameterization within a WRF framework: A Hurricane Sandy (2012) long-term track forecast perspective, Journal of Geophysical Research: Atmospheres, 120, 378-398, doi: 10.1002/2014JD022211, 2015.

Bhatia, K.T., Vecchi, G.A., Knutson, T. R., Murakami, H., Kossin, J., Dixon, K. W., and Whitlock, C. E.: Recent increases in tropical cyclone intensification rates, Nature Communications, 10, 635, doi: 10.1038/s41467-019-08471-z, 2019.

Bosart, L. F., Velden, C. S., Bracken, W. E., Molinari, J., and Black, P. G.: Environmental Influences on the rapid intensification of Hurricane Opal (1995) over the Gulf of Mexico, Monthly Weather Review, 128, 322-352, doi: 10.1175/1520-0493(2000)128<0322:EIOTRI>2.0.CO;2, 2000.

Bretherton, C. S., and Park, S.: A New Moist Turbulence Parameterization in the Community Atmosphere Model, Journal of Climate, 22(12), 3422-3448, doi: 10.1175/2008JCLI2556.1, 2009.

Chan, J. C. L, Duan, Y. H., and Shay, L. K.: Tropical Cyclone Intensity Change from a Simple Ocean-Atmosphere Coupled Model, Journal of the Atmospheric Sciences, 58, 154-172, doi: 10.1175/1520-0469(2001)058<0154:TCICFA>2.0.CO;2. 2001.

Chang, C.-C., and Wu, C.-C.: On the Processes Leading to the Rapid Intensification of Typhoon Megi (2010), Journal of the Atmospheric Sciences, 74, 1169-1200, doi: 10.1175/JAS-D-16-0075.1, 2017.

Chang, Y.-P., Yang, S.-C., Lin, K.-J., Lien, G.-Y., and Wu, C.-M.: Impact of Tropical Cyclone Initialization on Its Convection Development and Intensity: A Case Study of Typhoon Megi (2010), Journal of the Atmospheric Sciences, 77(2), 443-464, doi: 10.1175/JAS-D-19-0058.1, 2020.

Chen, H., and Zhang, D.-L.: On the rapid intensification of Hurricane Wilma (2005). Part II: Convective bursts and the upper-level warm core, Journal and Atmospheric Sciences, 70, 146-162, doi: 10.1175/JAS-D-12-062.1, 2013.

Chen, X. M., Xue, M., and Fang, J.: Rapid Intensification of Typhoon Mujigae (2015) under Differect Sea Surface Temperatures: Structural Changes Leading to Rapid Intensification, Journal of the Atmospheric Sciences, 75, 4313-4335, 2018.

Cione, J. J., and Uhlhorn, E. W.: Sea Surface Temperature Variability in Hurricanes: Implications with Respect to Intensity Change, Monthly Weather Review, 131(8), 1783-1796, doi: 10.1175//2562.1, 2003.

Črnivec, N., Smith, R. K., and Kilroy, G.: Dependence of tropical cyclone intensification rate on sea-surface temperature, Quarterly Journal of the Royal Meteorological Society, 142, 1618-1627, doi: 10.1002/qj.2752, 2016.

D'Asaro, E., Black, P. G., Centurioni, L. R., Chang, Y.-T., Chen, S. S., Foster, R. C., Graber, H. C., Harr, P., Hormann, V., Lien, R.-C., Lin, I.-I., Sanford, T. B., Tang, T.-Y., and Wu, C.-C.: Impact of Typhoons on the Ocean in the Pacific: ITOP, Bulletin of the American Meteorological Society, 95, 1405-1418, doi: 10.1175/BAMS-D-12-00104.1, 2014.

Eliassen, A., and Lystad, M.: On the Ekman layer in a circular vortex: a numerical and theoretical study, Geophysical Norvegica, 31, 1-16, doi: 10.1175/JAS-D-12-062.1, 1977.

https://doi.org/10.5194/egusphere-2023-61
Preprint. Discussion started: 8 March 2023

Emanuel, K.: An air-sea interaction theory for tropical cyclones. Part I: Steady-state maintenance, Journal of the Atmospheric Sciences, 3, 585-605, doi: 10. 1175/1520-0469(1986)043<0585:AASITF>2.0.CO;2, 1986.

Emanuel, K, DesAutels, C., Holloway, C., and Korty, R.: Environmental Control of Tropical Cyclone Intensity, Journal of the Atmospheric Sciences, 61, 843-858, doi: 10.1175/1520-0469(2004)061<0843:ECOTCI>2.0.CO;2, 2004.

Emanuel, K.: Thermodynamic control of hurricane intensity, Nature, 401, 665-669, doi: 10.1038/44326, 1999.

Emanuel, K.: Will global warming make hurricane forecasting more difficult? Bulletin of American Meteorological Society, 98, 495-501, 10.1175/BAMS-D-16-0134.1, 2017.

Elsberry, L. E., Chen, L. S., Davidson, J., Rogers, R., Wang, Y., and Wu, L.: Advances in Understanding and Forecasting Rapidly Changing Phenomena in Tropical Cyclones, Tropical Cyclone Research and Review, 2(1), 13-24, doi: 10.6057/2013TCRR01.02, 2013.

Fang, J., and Zhang, F. Q.: Contribution of Tropical Waves to the Formation of Supertyphoon Megi (2010), Journal of the Atmospheric Sciences, 74, 4387-4405, doi: 10.1175/JAS-D-15-0179.1, 2016.

Gall, R., Franklin, J., Marks, F., Rappaport, E. N., and Toepfer, F.: The Hurricane Forecast Improvement Project, Bulletin of the American Meteorological Society, 94, 329-343, doi: 10.1175/BAMS-D-12-00071.1, 2013.

Ge, X. Y., Shi, D. L., and Guan, L.: Monthly variations of tropical cyclone rapid intensification ratio in the western North Pacific, Atmospheric Science Letters, 19(4), e814, doi: 10.1002/asl.814, 2018.

Hazelton, A. T., Hart, R. E., and Rogers, R. F.: Analyzing Simulated Convective Bursts in Two Atlantic Hurricanes. Part II: Intensity Change due to Bursts. Monthly Weather Review, 145, 3095-3117, 10.1175/MWR-D-16-0268.1, 2017.

Hong, X. D., Chang, S. W., Raman, S., Shay, L. K., and Hodur, R.: The interaction between Hurricane Opal (1995) and a warm core ring in the Gulf of Mexico, Monthly Weather Review, 128, 1347-1365, doi: 10.1175/1520-0493(2000)1282.0.CO;2, 2000.

Holland, G. J.: The Maximum Potential Intensity of Tropical Cyclones, Journal of the Atmospheric Sciences, 54, 2519-2541, 10.1175/1520-0469(1997)054<2519:TMPIOT>2.0.CO;2, 1997.

Kaplan, J., and DeMaria, M., Large-scale characteristics of rapidly intensifying tropical cyclones in the North Atlantic basin, Weather and Forecasting, 18, 1093–1108, doi: 10.1175/1520-0434(2003)018<1093:lcorit>2.0.co;2, 2003.

Kanada, S., Tsujino, S., Aiki, H., Yoshioka, M. K., Miyazawa, Y., Tsuboki, K., and Takayabu, I.: Impacts of SST patterns on rapid intensification of Typhoon Megi (2010), Journal Geophysical Research: Atmospheres, 122, 13245-13262, doi: 10.1002/2017JD027252, 2017.

Kobashi, F., and Kubokawa, A.: Review on North Pacific Subtropical Countercurrents and Subtropical Fronts: role of mode waters in ocean circulation and climate, Journal of Oceanography, 68, 21-43, 10.1007/s10872-011-0083-7, 2012.

Krishnamurthy, V., and Shukla, J.: Intraseasonal and Interannual Variability of Rainfall over India. Journal of Climate, 13, 4366-4377. doi: 10.1175/1520-0442(2000)013<0001:IAIVOR>2.0.CO;2, 2000.

Latif, M., Neenlyside, N., and Bader, J.: Tropical sea surface temperature, vertical wind shear, and hurricane development, Geophysical Research Letters, 34, L01710, doi: 10.1029/2006GL027969, 2007.

https://doi.org/10.5194/egusphere-2023-61
Preprint. Discussion started: 8 March 2023

Law, K. T., and Hobgood, J. S.: A Statistical Model to Forecast Short-Term Atlantic Hurricane Intensity, Weather and Forecasting, 22, 967–980, doi: 10.1175/WAF1027.1, 2007.

Leipper, D. F., and Volgenau, D.: Hurricane Heat Potential of the Gulf of Mexico. Journal of Physical Oceanography, 2(3), 218-224, doi: 10.1175/1520-0485(1972)002<0218:HHPOTG>2.0.CO;2, 1972.

Lee, J.-D., and Wu, C.-C.: The Role of Polygonal Eyewalls in Rapid Intensification of Typhoon Megi (2010), Journal of the Atmospheric Sciences, 75(12), 4175-4199, doi: 10.1175/JAS-D-18-0100.1, 2018.

Lin, Y. L., and Colle, B. A.: A New Bulk Microphysical Scheme That Includes Riming Intensity and Temperature-Dependent Ice Characteristics, Monthly Weather Review, 139(3), 1013-1035, doi: 10.1175/2010MWR3293.1, 2011.

Liu, X., Li, Q., and Dai, Y.: Stronger vertical shear leads to earlier secondary eyewall formation in idealized numerical simulations, Geophysical Research Letters, 49, e2022GL098093, doi: 10.1029/2022GL098093, 2022.

Maclay, K. S., DeMariam, M., and Haar, T. H. V.: Tropical Cyclone Inner-Core Kinetic Energy Evolution, Monthly Weather Review, 136, 4882-4898, doi: 10.1175/2008MWR2268.1, 2008.

Ma, Z. H., Fei, J. F., Huang, X. G., and Cheng, X. P.: Contributions of Surface Sensible Heat Fluxes to Tropical Cyclone. Part I: Evolution of Tropical Cyclone Intensity and Structure, Journal of the Atmospheric Sciences, 72(1), 120-140, doi: 10.1175/JAS-D-14-0199.1, 2015.

Ma, Z. H., Fei, J. F., Liu, L., Huang, X. G., and Li, Y.: An Investigation of the Influences of Mesoscale Ocean Eddies on Tropical Cyclone Intensities, Monthly Weather Review, 145(4), 1181-1201, doi: 10.1175/MWR-D-16-0253.1, 2017.

McFarquhar, G. M., Jewett, B. F., Gilmore, M. S., Nesbitt, S. W., and Hsieh, T.: Vertical Velocity and Microphysical Distributions Related to Rapid Intensification in a Simulation of Hurricane Dennis (2005), Journal of Atmospheric and Sciences, 69, 3515-3534, doi: 10.1175/JAS-D-12-016.1, 2012.

Mei, W., and Xie, S.P.: Intensification of landfalling typhoons over the northwest Pacific since the late 1970s, Nature Geoscience, 9, 753-757, doi: 10.1038/ngeo2792, 2016.

Montgomery, M. T., Snell, H. D., and Yang, Z.: Axisymmetric Spindown Dynamics of Hurricane-like Vortices, Journal of Atmospheric Sciences, 58, 421-435, doi: 10.1175/1520-0469(2001)058<0421:ASDOHL>2.0.CO;2, 2001.

Montgomery, M. T., Zhang, J. A., and Smith, R. K.: An analysis of the observed low-level structure of rapidly intensifying and mature Hurricane Earl (2010), Quarterly Journal of the Royal Meteorological Society, 138, 1-14, 10.1002/qj.2283, 2013.

Pun, I.-F., Lin, I.-I., Lien, C.-C., and Wu, C.-C.: Influence of the Size of Supertyphoon Megi (2010) on SST Cooling, Monthly Weather Review, 146, 661-677, doi: 10.1175/MWR-D-17-0044.1, 2018.

Ren, X. J., Yang, X. Q., and Sun, X. G.: Zonal Oscillation of Western Pacific Subtropical High and Subseasonal SST Variations during Yangtze Persistent Rainfall Events, Journal of Climate, 26, 8929-8946, doi: 10.1175/JCLI-D-12-00861.1, 2013.

Riemer, M., Montgomery, M. T., and Nicholls, M.: Further examination of the thermodynamic modification of the inflow layer of tropical cyclones by vertical wind shear. Atmospheric Chemistry and Physics, 13, 327-346, doi: 10.5194/acp-13-327-2013, 2013.

https://doi.org/10.5194/egusphere-2023-61
Preprint. Discussion started: 8 March 2023

Rogers, R.: Convective-Scale Structure and Evolution during a High-Resolution Simulation of Tropical Cyclone Rapid Intensification, Journal of the Atmospheric Sciences, 67(1), 44-70, doi: 10.1175/2009JAS3122.1, 2010.

Rogers., R. F., Reason, P. D., and Lorsolo, S.: Airborne Doppler Observations of the Inner-Core Structural Differences between Intensifying and Steady-State Tropical Cyclones, Monthly Weather Review, 141, 2970-2991, doi: 10.1175/MWR-D-12-00357.1, 2013.

Rogers, R. F., Reasor, P. D., and Zhang, J. A.: Multiscale Structure and Evolution of Hurricane Earl (2010) during Rapid Intensification, Monthly Weather Review, 143, 536-562, doi: 10.1175/MWR-D-14-00175.1, 2015.

Shay, L. K., Goni, G. J., and Black, P. G.: Effects of a Warm Oceanic Feature on Hurricane Opal, Monthly Weather Review, 128(5), 1366-1383, doi: 10.1175/1520-0493(2000)128<1366:EOAWOF>2.0.CO;2, 2000.

Singh, V. K., Roxy, M. K., and Deshpande, M.: Role of warm ocean conditions and the MJO in the genesis and intensification of extremely severe cyclone Fani, 11, 3607, doi: 10.1038/s41598-021-82680-9, 2021.

Smith, R. K., and Montgomery, M. T.: Toward Clarity on Understanding Tropical Cyclone Intensification, Journal of the Atmospheric Sciences, 72, 3020-3031, doi: 10.1175/JAS-D-15-0017.1, 2015.

Sun, Y., Zhong, Z., Li, L., Ha, Y., and Sun, Y. M.: The opposite effects of inner and outer sea surface temperature on tropical cyclone intensity, Journal of Geophysical Research: Atmospheres, 119, 293-2208, doi: 10.1002/2013JD021354, 2014.

Tao, C., and Jiang, H. Y.: Distributions of Shallow to Very Deep Precipitation-Convection in Rapidly Intensifying Tropical Cyclones, Journal of Climate, 28, 8791-8824, doi: 10.1175/JCLI-D-14-00448.1, 2015.

Tao, D. D., and Zhang, F. Q.: Evolution of Dynamic and Thermodynamic Structures before and during Rapid Intensification of Tropical Cyclones: Sensitivity to Vertical Wind Shear, Monthly Weather Review, 147, 1171-1191, doi: 10.1175/MWR-D-18-0173.1, 2019.

Vitart, F., and Robertson, A.W.: The sub-seasonal to seasonal prediction project (S2S) and the prediction of extreme events. Nature partner journals, Climate and Atmospheric Science, 1, 3, doi: 10.1038/s41612-018-0013-0, 2018.

Wang, H., and Wang, Y. Q.: A Numerical Study of Typhoon Megi (2010). Part I: Rapid Intensification. Monthly Weather Review, 142, 29-48, doi: 10.1175/MWR-D-13-00070.1, 2014.

Wang, X.-D., Wang, C.-Z., Zhang, L.-P., and Wang, X.: Multidecadal Variability of Tropical Cyclone Rapid Intensification in the Western North Pacific, Journal of Climate, 28(9), 3806-3820, doi: 10.1175/JCLI-D-14-00400.1, 2015.

Wang, C. Z., Wang, X. D., Weisberg, R. H., and Black, M. L.: Variability of tropical cyclone rapid intensification in the North Atlantic and its relationship with climate variations, Climate Dynamics, 49, 367-3645, doi: 10.1007/s00382-017-3537-9, 2017.

Wang, B., and Zhou, X.: Climate variation and prediction of rapid intensification in tropical cyclones in the western North Pacific, Meteorology and Atmospheric Physics, 99, 1-16. 2007, doi: 10.1007/s00703-006-0238-z, 2008.

https://doi.org/10.5194/egusphere-2023-61
Preprint. Discussion started: 8 March 2023

Wu, C.-C., Tu, W.-T., Pun, I.-F., Lin, I.-I., and Peng, M. S.: Tropical cyclone-ocean interaction in Typhoon Megi (2010) - A Synergy Study Based on ITOP Observations and Atmosphere-ocean Coupled Model Simulations, Journal Geophysical Research: Atmospheres, 121, 153-167, doi: 10.1002/2015JD024198, 2016.

Xu, J., and Wang, Y. Q.: Dependence of Tropical Cyclone Intensification Rate on Sea Surface Temperature, Storm Intensity, and Size in the Western North Pacific, Weather and Forecasting, 33, 523-537, doi: 10.1175/WAF-D-17-0095.1, 2018.

Yang, M.-J., Zhang, D.-L., and Huang, H.-L.: A modeling study of Typhoon Nari (2001) at landfall. Part I: Topographic effects, Journal of the Atmospheric Sciences, 5, 3095-3115, doi: 10.1175/2008JAS2453.1, 2008.

Zhao, H. K., Duan, X. Y., Raga, G. B., and Klotzbach, P. J.: Changes in Characteristics of Rapidly Intensifying Western North Pacific Tropical Cyclones Related to Climate Regime Shifts, Journal of Climate, 31, 8163-8179, doi: 10.1175/JCLI-D-18-0029.1, 2018.

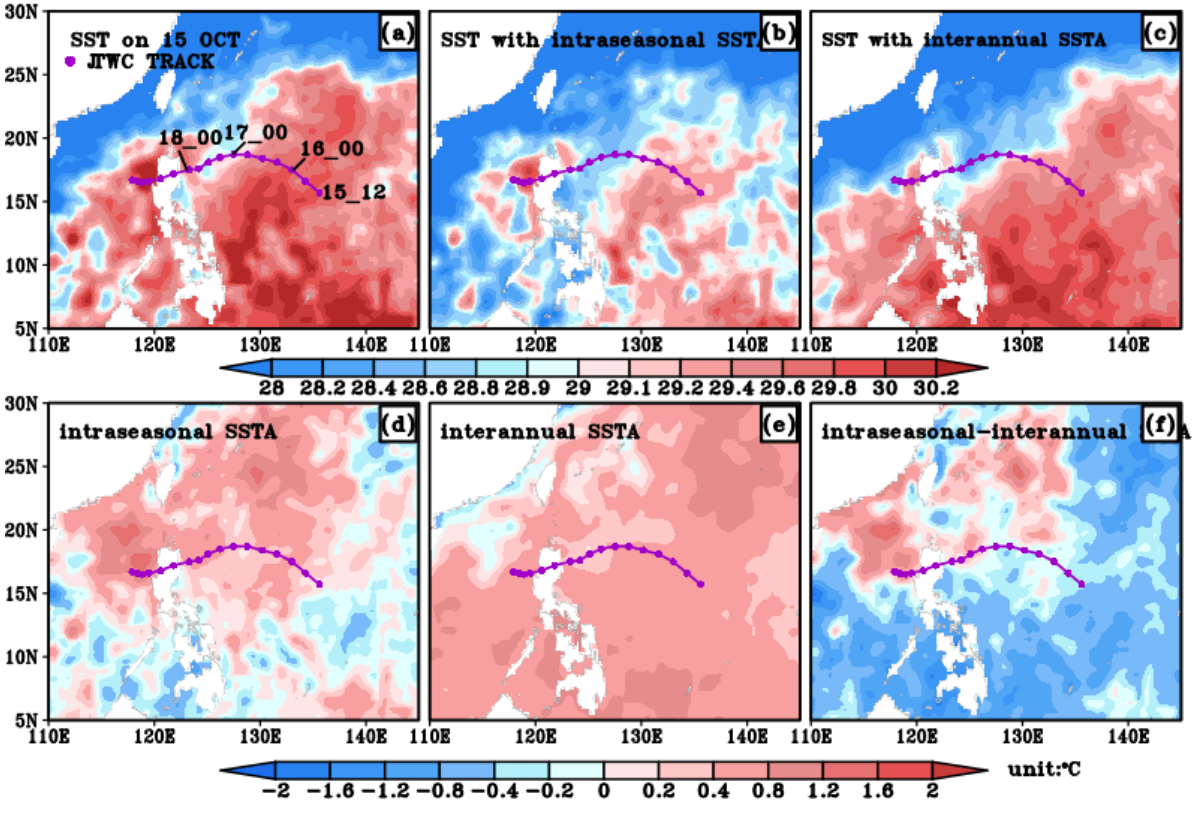

Figure 1. The SST and SSTA during the track of Megi on 15 OCT. Panel (a)-(f) is AVHRR daily SST, SST with intraseasonal SSTA, SST with interannual SSTA, intraseasonal SSTA, interannual SSTA, and the difference between intraseasonal and interannual SSTA, respectively (unit: ˚C). The track points is denoted by 6h interval from 12 UTC 15 OCT to 00 UTC 19 OCT.

https://doi.org/10.5194/egusphere-2023-61
Preprint. Discussion started: 8 March 2023

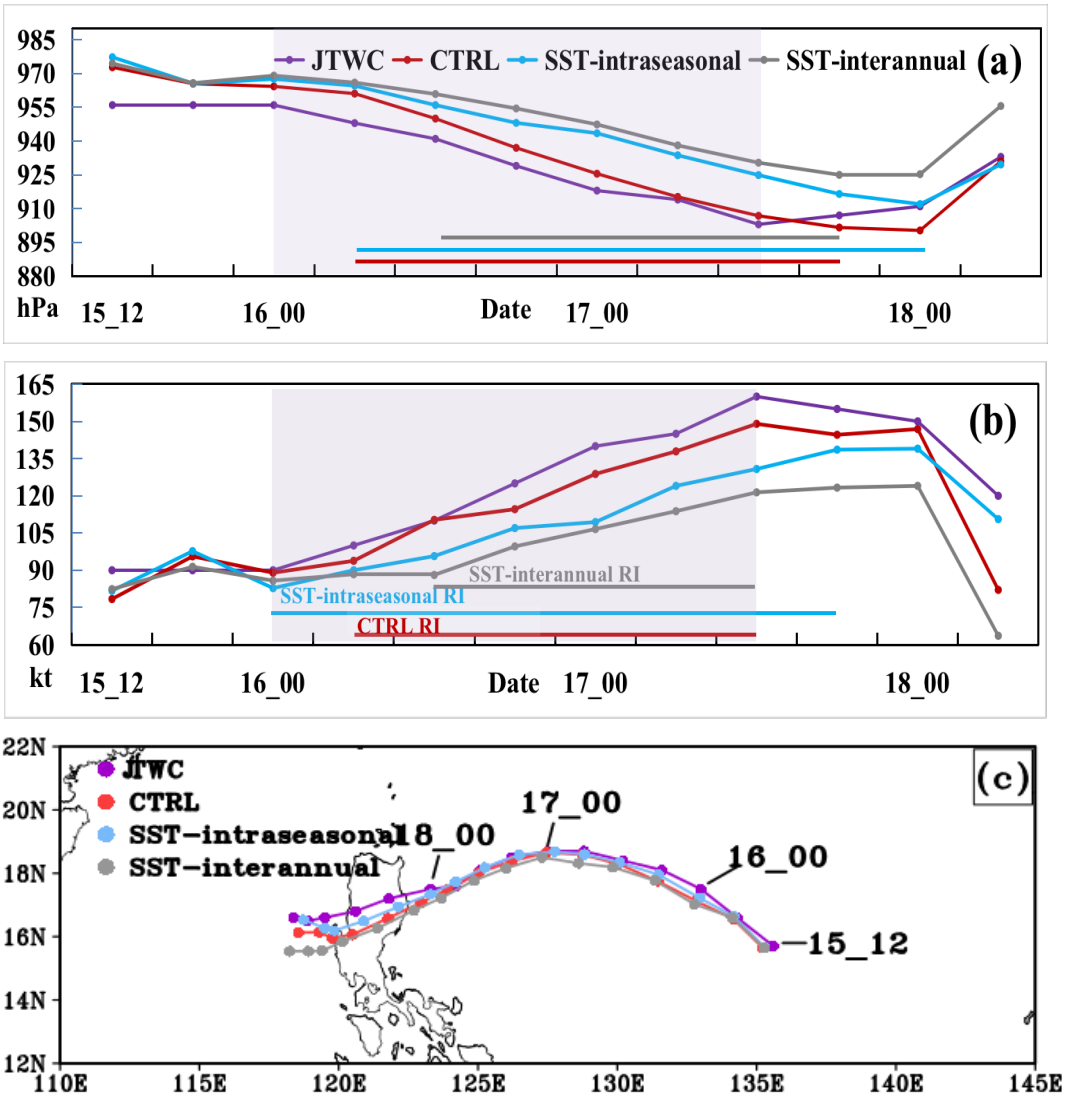

Figure 2. The simulated and observed intensity and track of Typhoon Megi. Panel (a) denotes the evolution of TC minimum CSLP (hPa). Panel (b) is for TC MWS (kt). The purple shaded region indicates the RI period of JTWC. Panel (c) shows the TC track.

https://doi.org/10.5194/egusphere-2023-61
Preprint. Discussion started: 8 March 2023

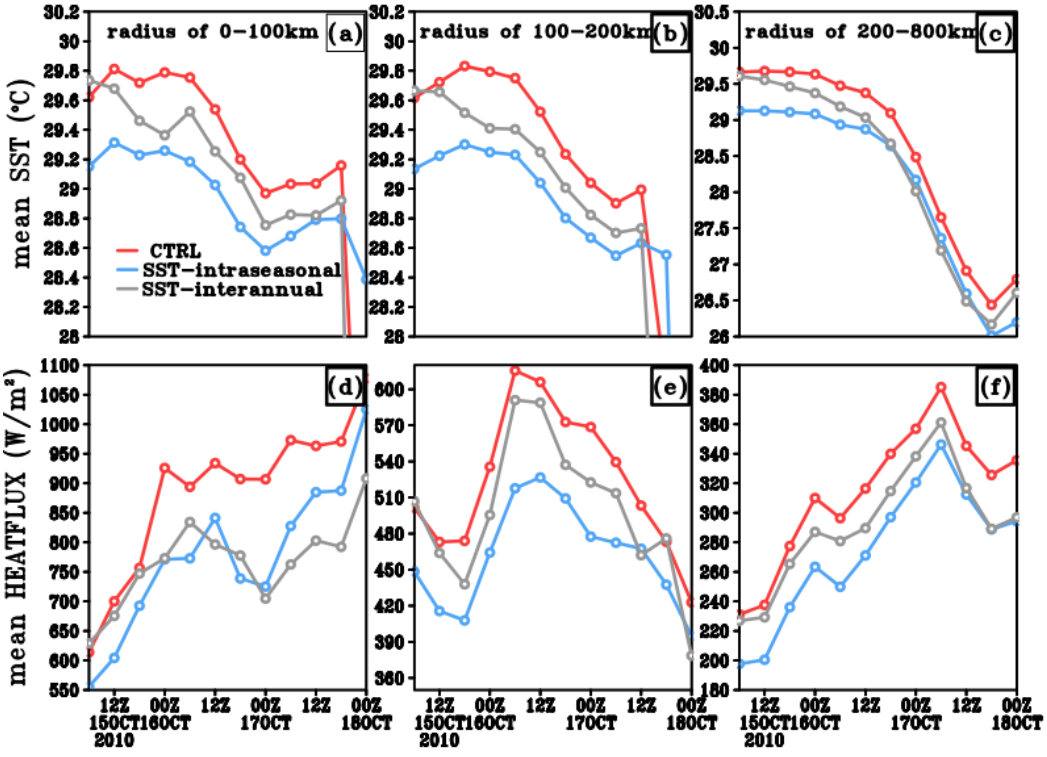

Figure 3. Evolution of horizontal averaged SST and air-sea interface heat flux. Panel (a)-(c) is time series of averaged SST from the radius of 0-100km, 100-200km and 200-800km, respectively (˚C). Panel (d)-(f) is same as (a)-(c) but for heat flux (Wm-2).

https://doi.org/10.5194/egusphere-2023-61
Preprint. Discussion started: 8 March 2023

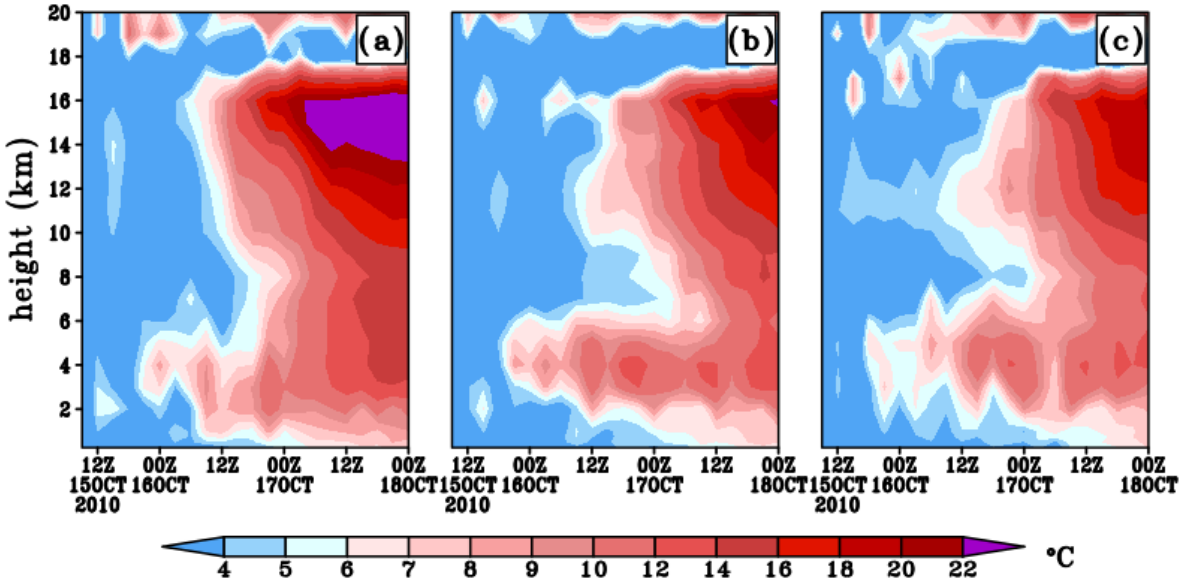

555 **Figure 4. Time-height plots for the potential temperature anomaly above the surface center. Panels (a)-(c) shows the result of CTRL, SST-intraseasonal and SST-interannual, respectively. The reference state for the potential temperature anomaly is the potential temperature profile at 0900 UTC 15 OCT (°C).**

https://doi.org/10.5194/egusphere-2023-61
Preprint. Discussion started: 8 March 2023

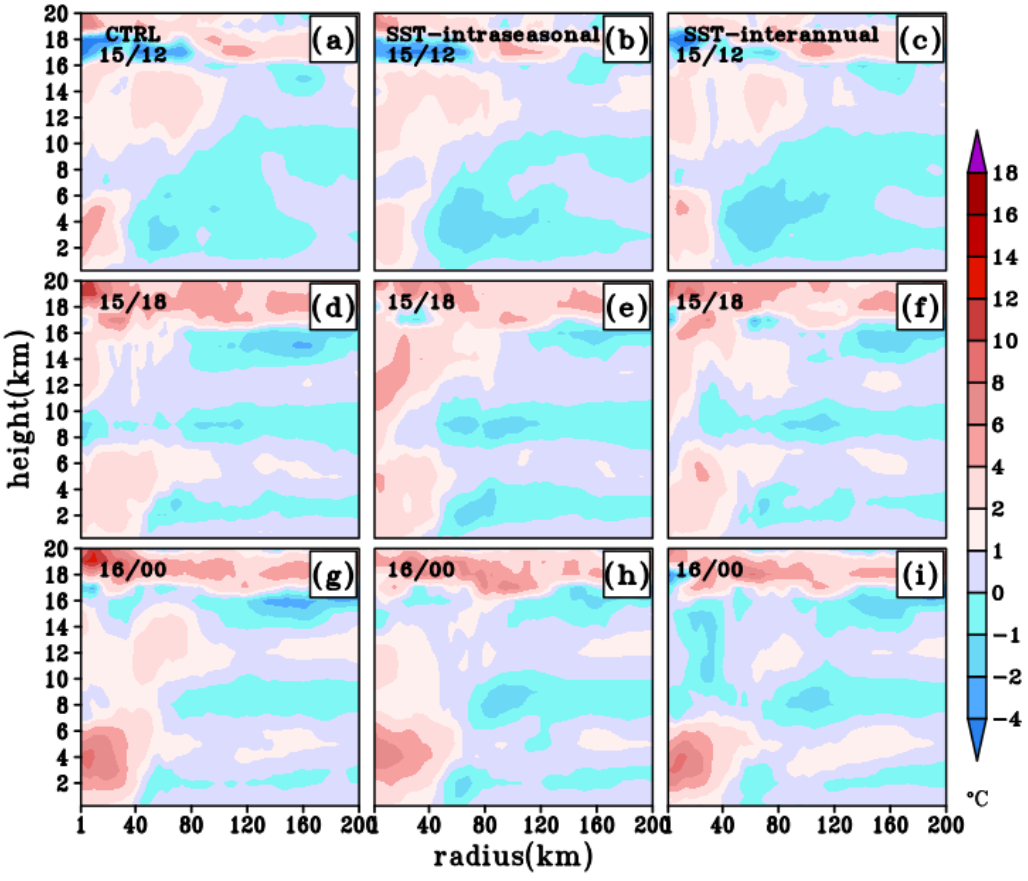

Figure 5. Height-raidus plots for TC azimuthally averaged potential temperature anomaly before TC RI. The reference state for the potential temperature anomaly is the potential temperature profile at 0900 UTC 15 OCT (°C).

https://doi.org/10.5194/egusphere-2023-61
Preprint. Discussion started: 8 March 2023

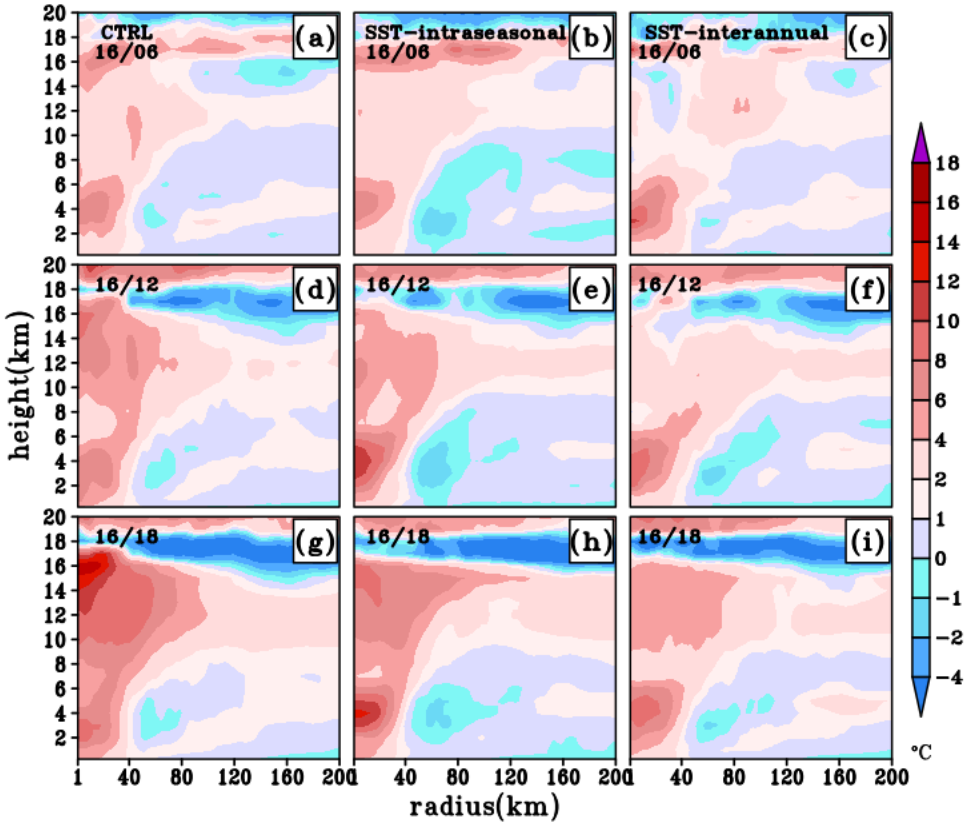

Figure 6. Same as Figure 5 but on 16 OCT. (unit: °C)

https://doi.org/10.5194/egusphere-2023-61
Preprint. Discussion started: 8 March 2023

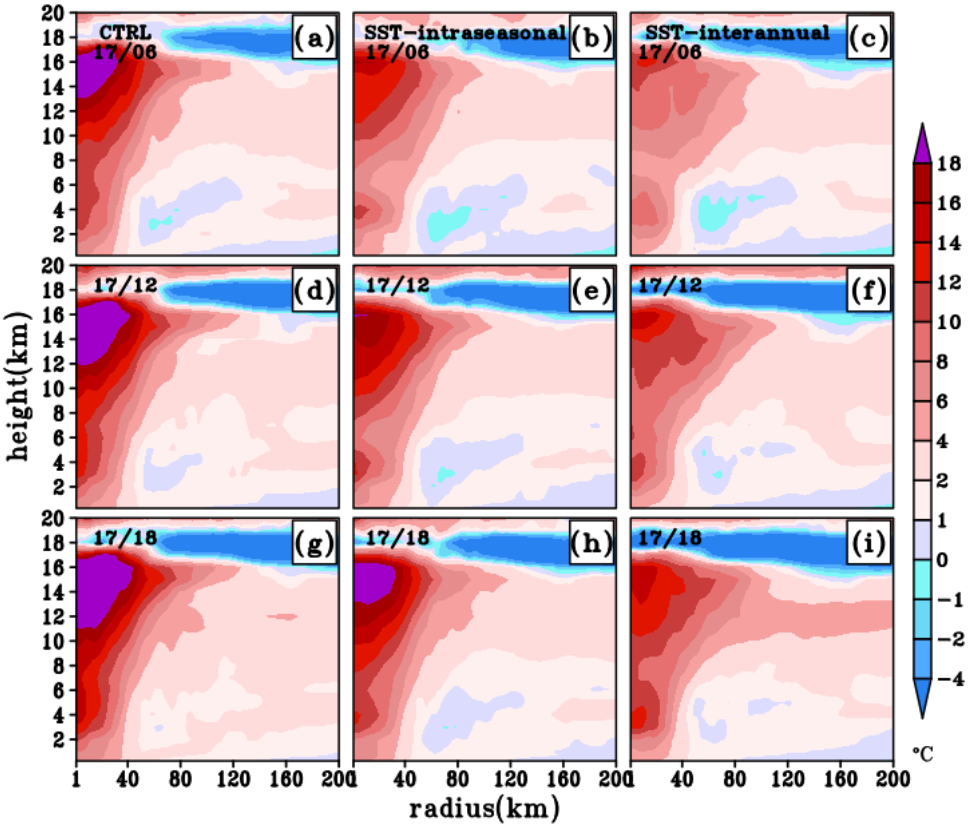

Figure 7. Same as Figure 6 but on 17 OTC. (°C)

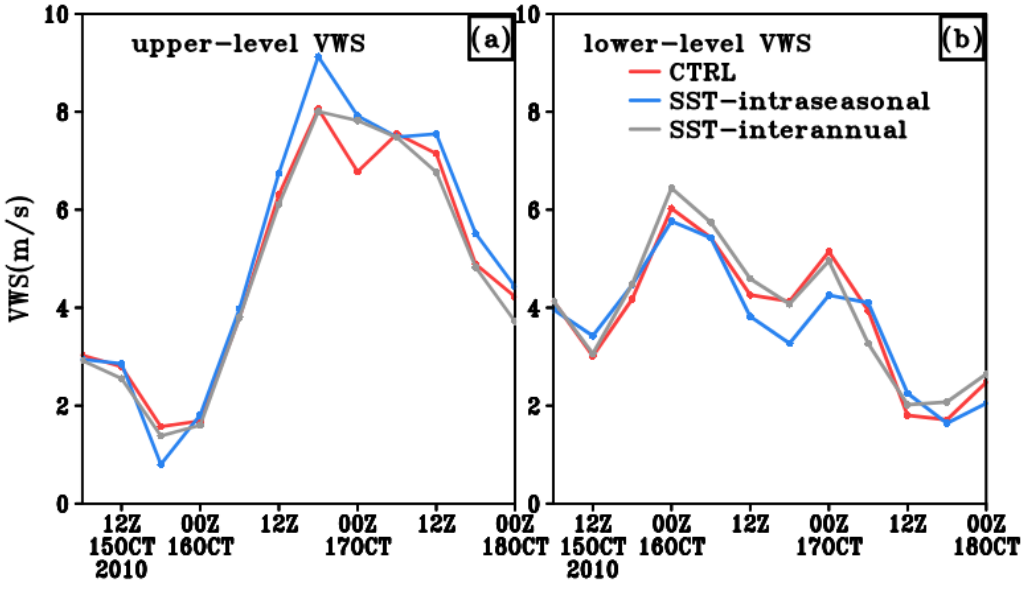

565

https://doi.org/10.5194/egusphere-2023-61
Preprint. Discussion started: 8 March 2023

Figure 8. Comparison of the two-level VWS. The upper-level and lower-level VWS is 200-800 km area-averaged differences of wind vectors between 14 and 8 km, and between 8 and 2 km, respectively (ms-1).

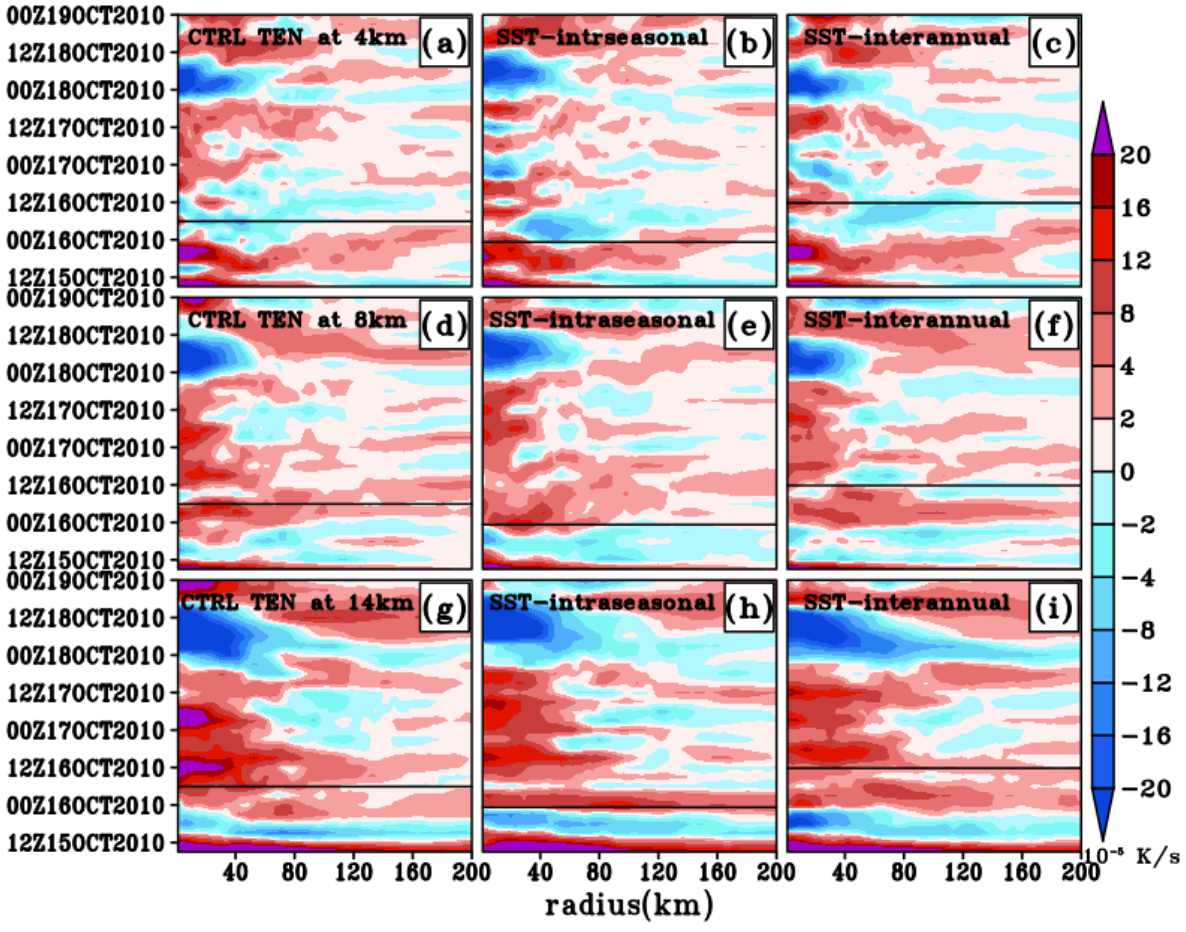

Figure 9. Time-radius plots of azimuthally averaged local tendency of potential temperature (units: 10-3Ks-1) at the height of 4 km (a-c), 8 km (d-f), and 14 km (g-i), respectively. Black line denotes the time of RI onset.

https://doi.org/10.5194/egusphere-2023-61
Preprint. Discussion started: 8 March 2023

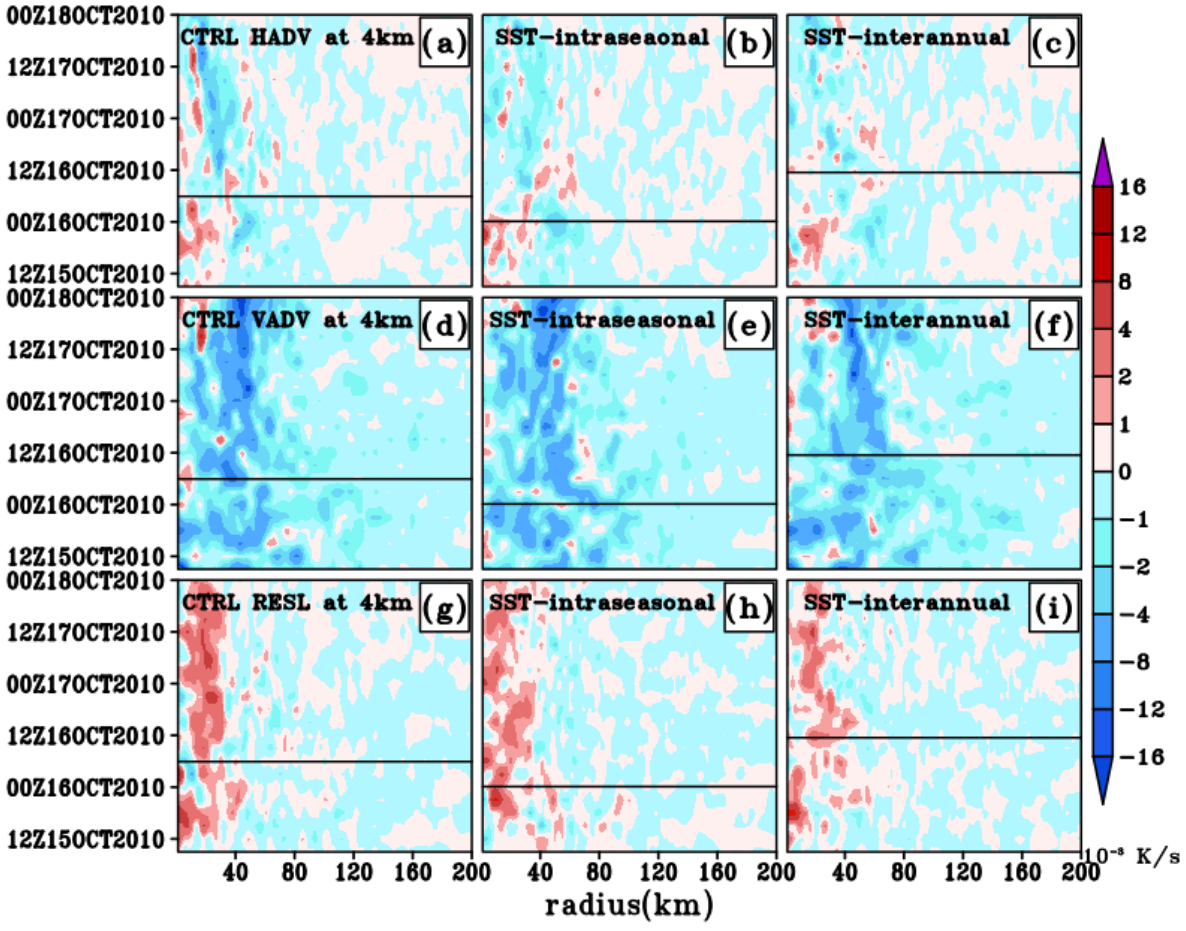

Figure 10. Time-radius plots of azimuthally averaged contribution of potential temperature budget terms (HADV, VADV and RESI) at 4 km height (units: 10-3Ks-1). Black line denotes the RI onset.

https://doi.org/10.5194/egusphere-2023-61
Preprint. Discussion started: 8 March 2023

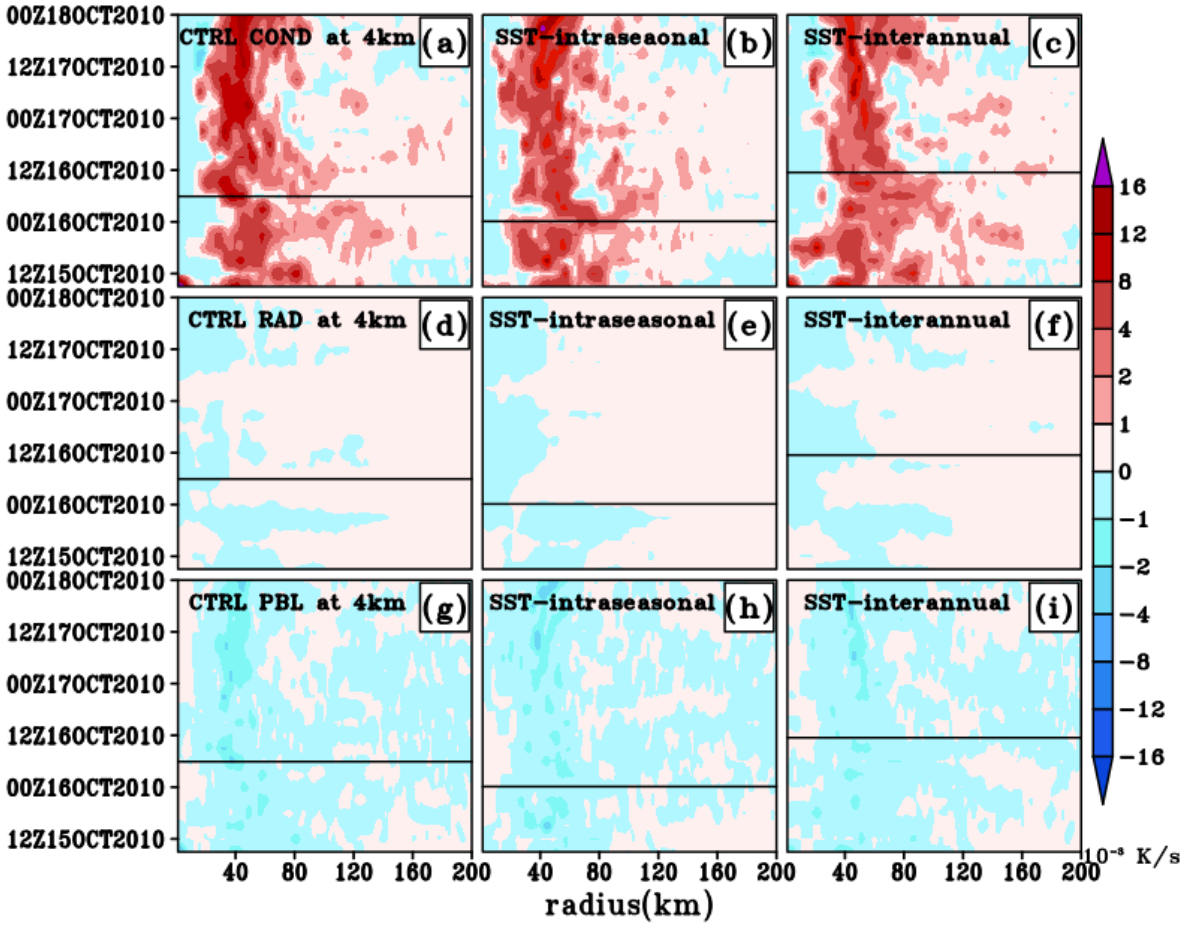

575 **Figure 11. Same as Figure 10 but for the terms of COND, RAD and PBL.**

https://doi.org/10.5194/egusphere-2023-61
Preprint. Discussion started: 8 March 2023

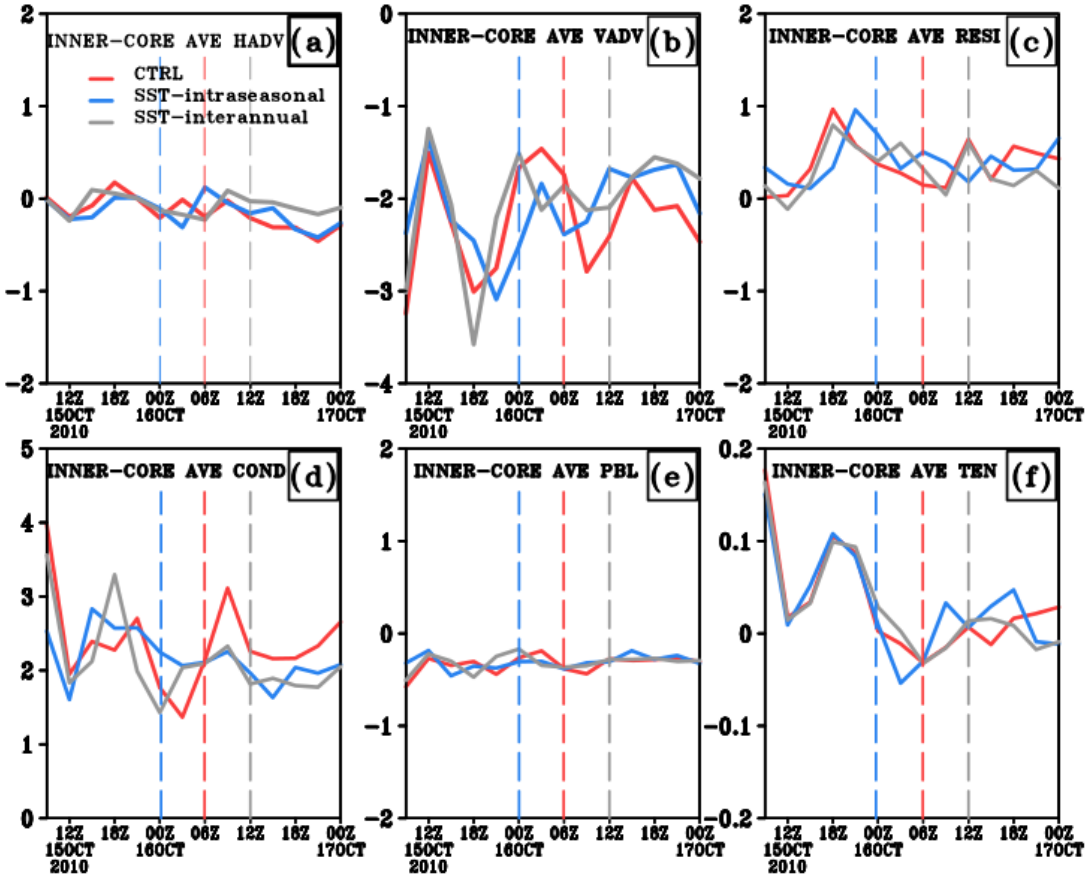

Figure 12. Evolution of tangential potential temperature budget terms at 4 km height, averaged inside TC inner-core region (units: 10-3Ks-1). Red, blue, and grey dashed lines denote the RI onset of CTRL, SST-intraseasonal and SST-interannual, respectively.

https://doi.org/10.5194/egusphere-2023-61
Preprint. Discussion started: 8 March 2023

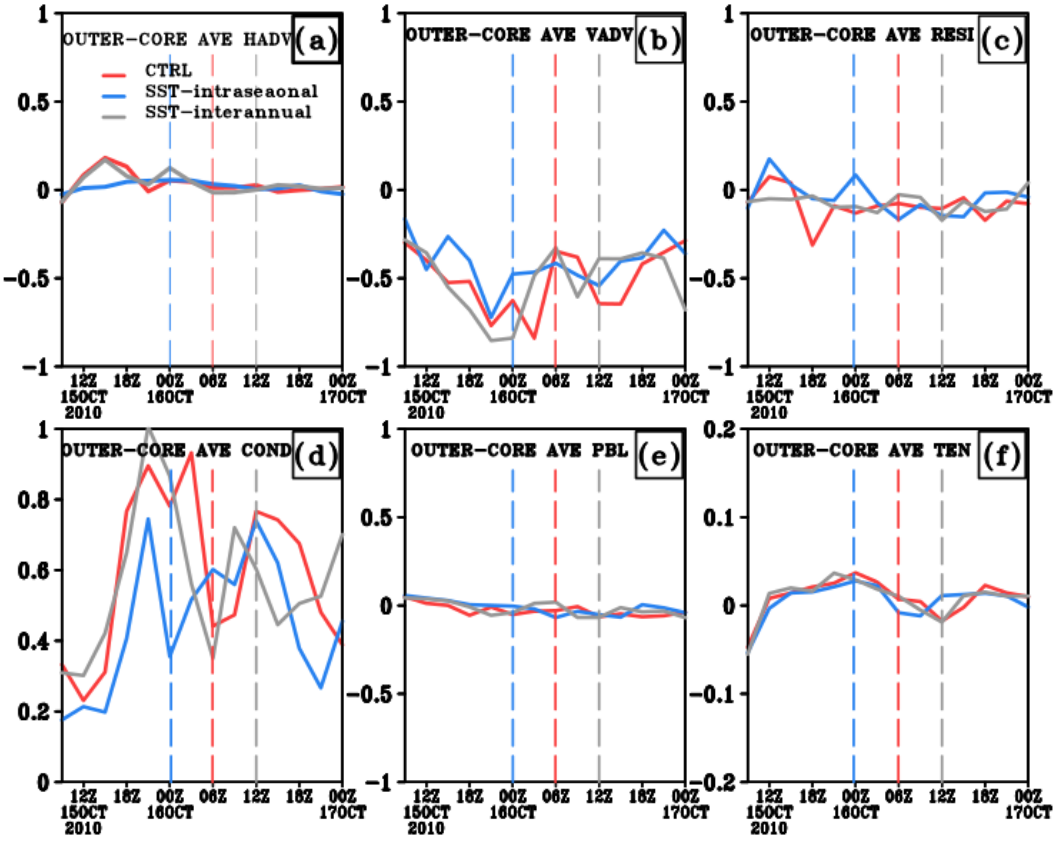

580 **Figure 13. Same as Figure 12 but for TC outer-core region.**

https://doi.org/10.5194/egusphere-2023-61
Preprint. Discussion started: 8 March 2023

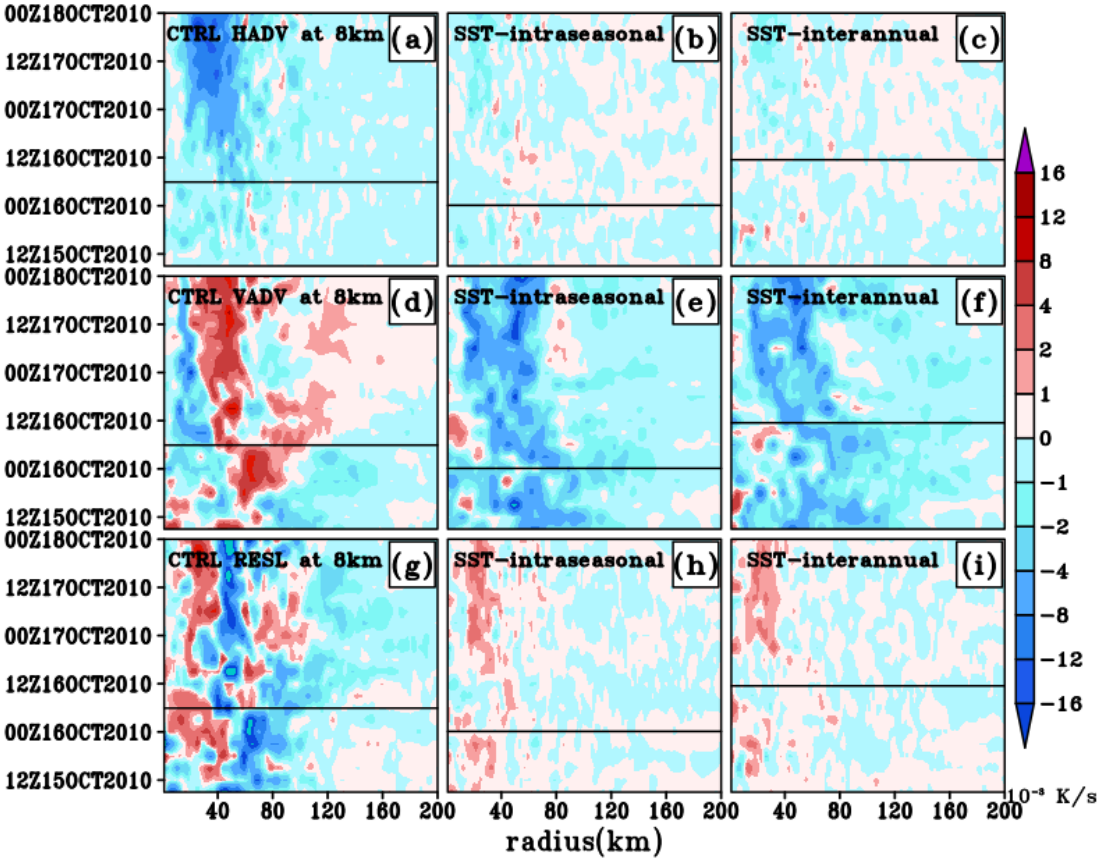

Figure 14. Time-radius plots of azimuthally averaged contribution of potential temperature budget terms (HADV, VADV and RESI) at 8 km height (units: 10-3Ks-1). Black line denotes the time of TC RI onset.

https://doi.org/10.5194/egusphere-2023-61
Preprint. Discussion started: 8 March 2023

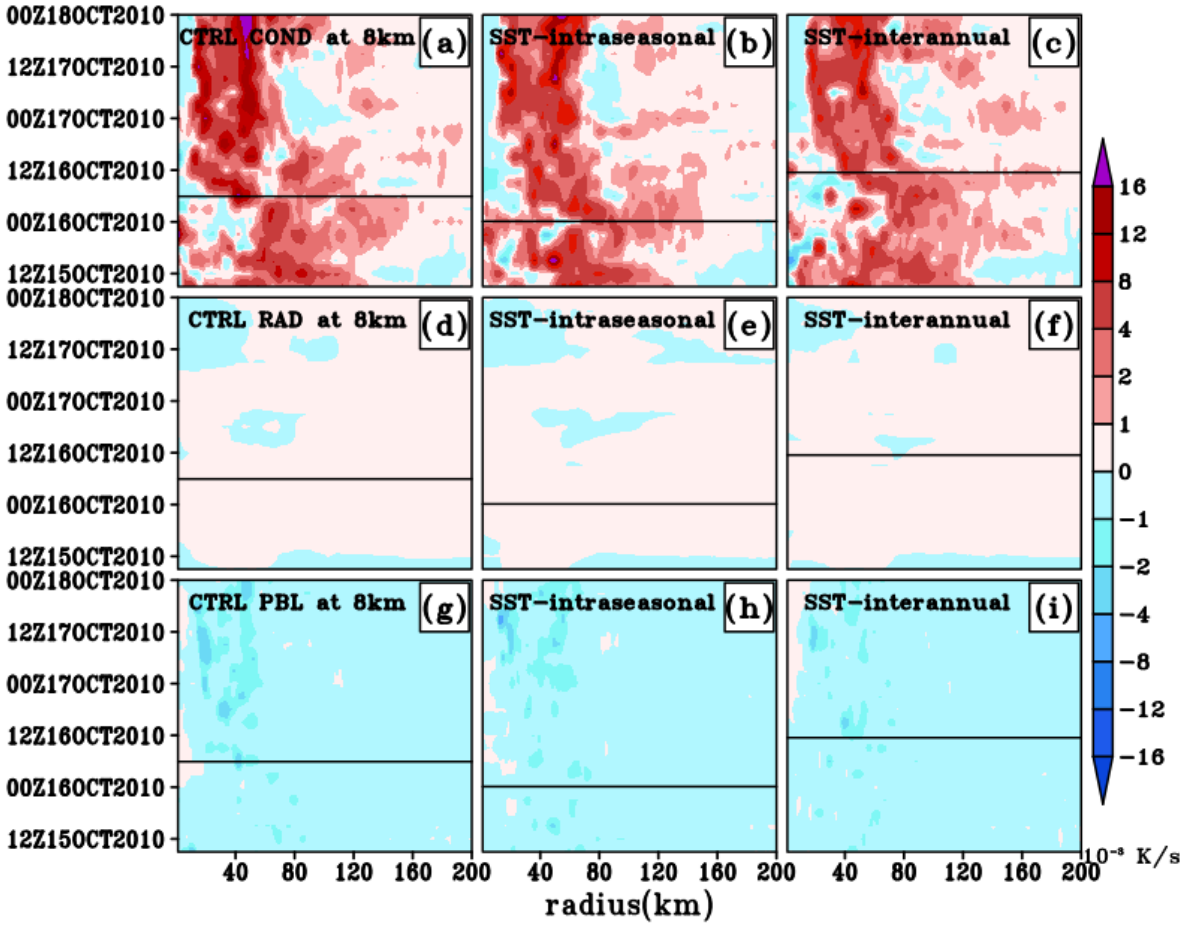

585 **Figure 15. Same as Figure 14 but for the terms of COND, RAD and PBL.**

https://doi.org/10.5194/egusphere-2023-61
Preprint. Discussion started: 8 March 2023

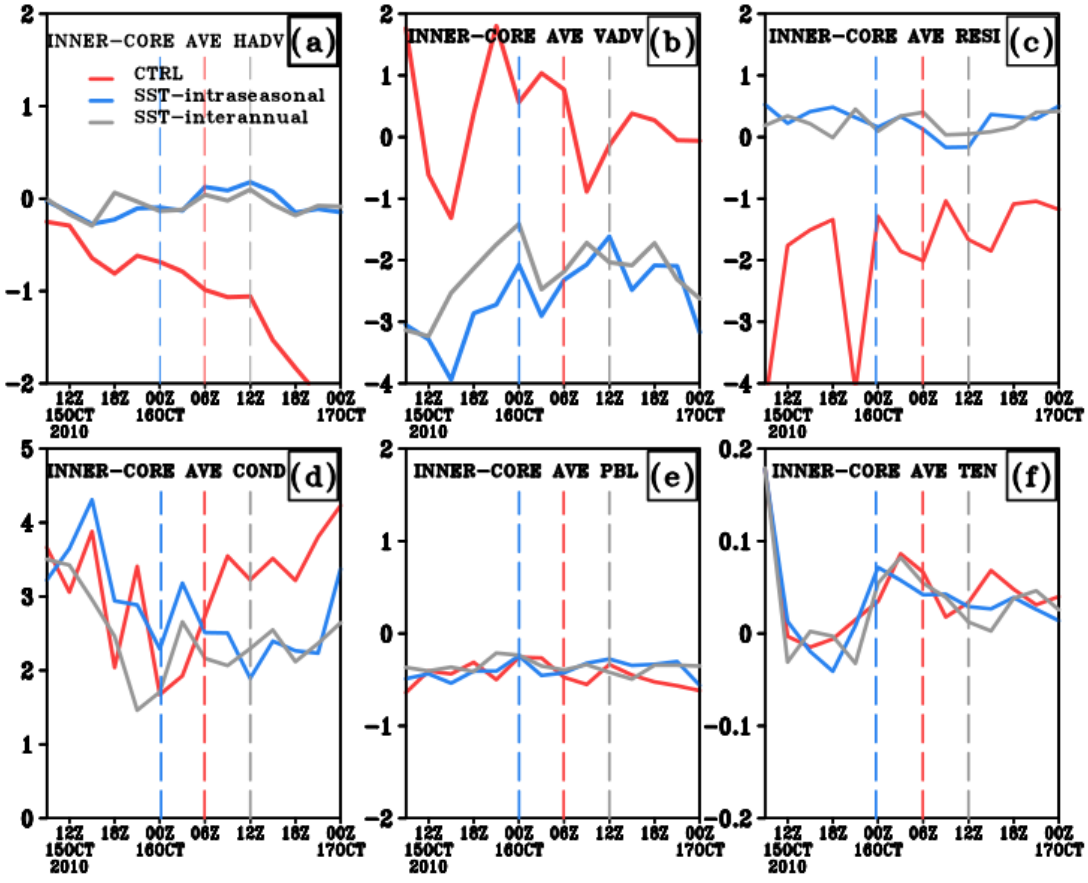

Figure 16. Evolution of potential temperature budget terms at 8 km height, averaged inside TC inner-core region (units: 10-3Ks-1). Red, blue and grey dashed lines denote the RI onset of CTRL, SST-intraseasonal and SST-interannual, respectively.

https://doi.org/10.5194/egusphere-2023-61
Preprint. Discussion started: 8 March 2023

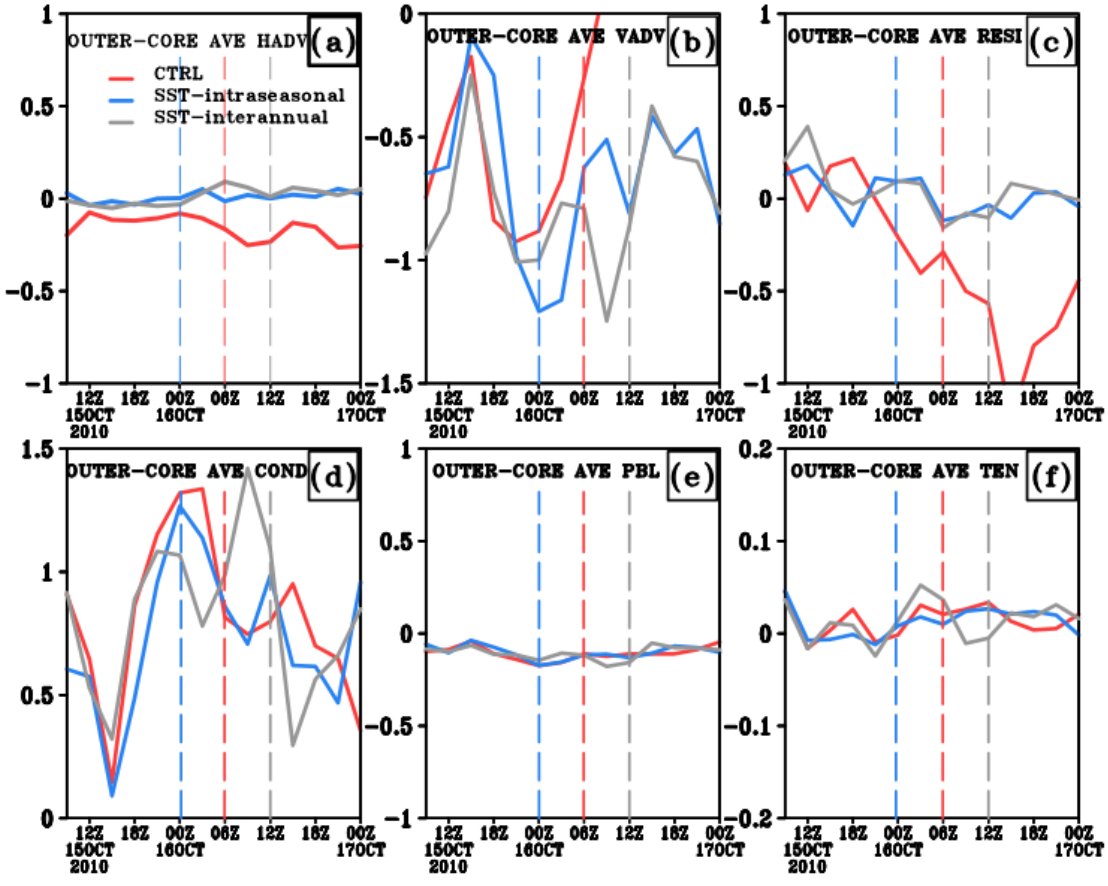

590 **Figure 17. Same as Figure 16, but for the outer-core region.**

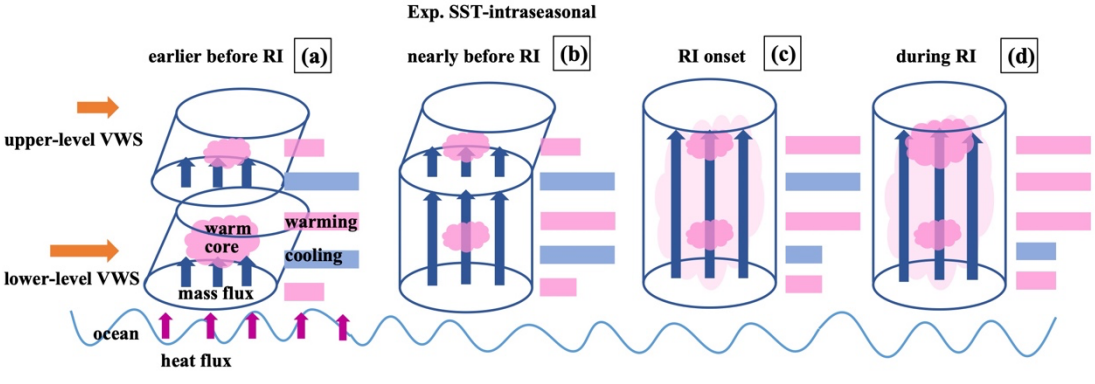

https://doi.org/10.5194/egusphere-2023-61
Preprint. Discussion started: 8 March 2023

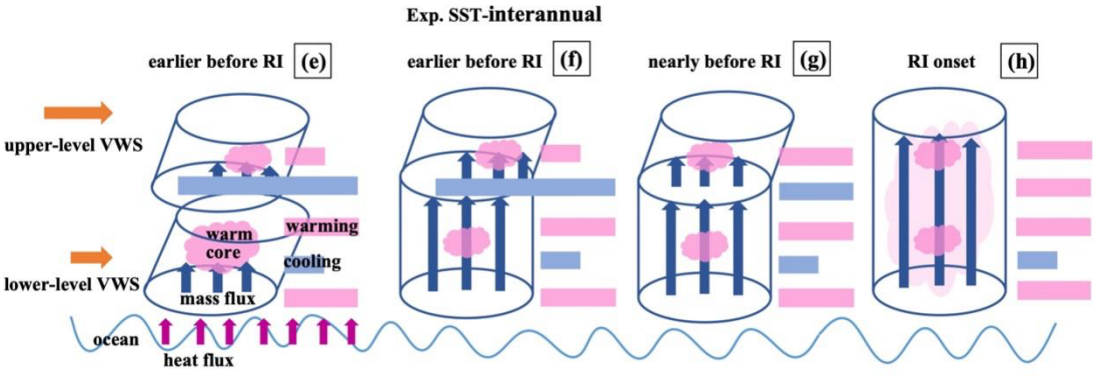

Figure 18. The conceptual model of Megi RI onset in SST-intraseasonal and SST-interannual. The length of shear arrow indicates shear strength. The length of TC outer-core cooling (warming) band represents the position and amplitude of the temperature change relative to the initial time.